Evaluation of Distortion and Residual Stresses Caused by Heat Treatment of Cast Aluminum Alloy Components

by

Chang-Kai (Lance) Wu

A Dissertation

Submitted to the faculty

Of the

WORCESTER POLYTECHINC INSTITUTE

In partial fulfillment of the requirements of the

Degree of Master of Science

in

Materials Science and Engineering

by

APPROVED:

Advisor: Makhlouf M. Makhlouf

Richard D. Sisson J r. Director of Material Science and Engineering

ABSTRACT

The objective of this research was to develop and verify a mathematical model that enables the prediction of the effects of heat treatment on cast aluminum alloy components. The model, which uses the commercially available software (ABAQUS), predicts dimensional changes, distortion, and residual stresses in heat treated components.

An extensive database is developed for an example aluminum alloy (A356) and includes the mechanical, physical, and thermal properties of the alloy all as functions of temperature. The database is obtained through calculations and measurements made on A356 alloy specimens. In addition, boundary conditions – in the form of heat transfer coefficients for each of the heat treatment steps - are obtained from measurements performed with a special quenching system developed at the Center for Heat Treating Excellence at WPI.

The database and boundary conditions were used in the software to predict the dimensional changes, distortions, and residual stresses that develop in a commercial A356 cast component that is subjected to a standard commercial heat treating cycle.

In order to verify the accuracy of the software predictions, the predictions were compared to their measured counterparts, where dimensional changes and distortion were measured with a coordinate measuring machine, and residual stresses were measured with x-ray diffraction.

ACKNOWLEDGEMENTS

I have worked with a great number of people whose contribution in various ways to my research and the making of this thesis deserve special mention. It is a pleasure to convey my gratitude to them all in my humble acknowledgement.

I am deeply grateful to Professor Makhlouf M. Makhlouf for giving me the opportunity to work with him on this project. It has been an honor to be his student. I would like to deliver my special gratitude to him for his advice, time, ideas and supervision from the very beginning to the end of this research, as well as for sharing his unique experience with me throughout the work. His words of encouragement and motivation came a long way in bringing this work to completion. I would like to thank Professor Diran Apelian for his advice and guidance throughout these years. He has been a great help not only in my academic performance, but also in my personal development. It is my pleasure also to pay tribute to all the WPI faculty and staff.

I deeply appreciate my family, especially my mother. She devoted her life to me, and sincerely raised me with her caring and gentle love. Collective and individual acknowledgements are also due to colleagues, classmates and friends whose enthusiasm and support in one way or another was helpful and memorable. The group at ACRC has contributed immensely to my personal and professional experience at WPI. The team has been a wonderful source of friendships, good advice and collaboration.

I want to thank the Metals Processing Institute and the Department of Materials

Science and Engineering at WPI who gave me the opportunity to be a part of them. Finally, I thank everyone who supported and believed in me, and I express my apology to anyone who I did not mention personally.

Chang-Kai (Lance) Wu

Worcester Polytechnic Institute

Metals Processing Institute

April, 2009

TABLE OF CONTENTS

LIST OF FIGURES

LIST OF TABLES

1. Introduction

The mechanical properties of aluminum alloy castings can be greatly improved by a precipitation hardening heat treatment. Typically, this heat treatment consists of three steps: (1) solutionizing, (2) quenching, and (3) aging; and is performed by first heating the casting to and maintaining it at a temperature that is a few degrees lower than the solidus temperature of the alloy in order to form a single-phase solid solution. The casting is then rapidly quenched in a cold (or warm) fluid in order to form a supersaturated non-equilibrium solid solution. The casting is then aged by reheating it to a temperature that allows the controlled nucleation and growth of strengthening precipitate(s) to occur thereby increasing the alloy's yield strength [1].

Aluminum alloy cast components experience considerable changes during heat treatment. These include changes in mechanical properties, in dimensions, in magnitude and sense of residual stresses, and in metallurgical phase composition. Residual stresses often adversely affect the mechanical properties of the cast component. They are caused by differing rates of cooling during quenching and depend on the differential rate of cooling, section thickness, and material strength. In addition to the completely reversible changes that are caused by thermal expansion and contraction, metallic components experience permanent dimensional changes during heat treatment. These permanent changes can be classified into three main groups based on their origin. These are (1) Dimensional changes with mechanical origins which include dimensional changes caused by stresses developed by external forces, dimensional changes arising from thermally induced stresses, and dimensional changes

caused by relaxation of residual stresses. (2) Dimensional changes due to quenching which are dimensional changes that occur during quenching or that result from stresses induced by quenching. (3) Dimensional changes with metallurgical origins which include dimensional changes caused by re-crystallization, solution and precipitation of alloying elements, and phase transformations.

Since most of the quality assurances criteria that cast components have to meet include prescribed minimum mechanical properties and compliance with dimensional tolerances, it is necessary for casters to be able to accurately predict these changes in order to take appropriate measures to insure the production of parts that meet the required specifications. Satisfactory response to heat treatment is often gauged by the ability of the component to be heat treated to a desired microstructure, hardness and strength level without undergoing cracking, distortion or excessive dimensional changes. Most of the products manufactured today are designed using sophisticated computer models and finite element analysis (FEA). These models are built on sound physical concepts and mathematical equations. Several commercially available software packages are capable of predicting the heat treatment response of wrought steels [2, 3]. One good example is DANTE [4], a subroutine that has an extensive material database and is used with ABAQUS[1] for heat treatment and cooling process simulations of steels. However, none of the commercially available software packages is able to accurately predict the response of cast aluminum alloy components to heat treatment.

This work focused on developing a computer model for predicting (1) residual stresses, (2)

[1]ABAQUES is marketed by Slovia, Inc. Rhode Island, USA.

dimensional changes that have mechanical origins. Dimensional changes that have metallurgical origins are not addressed here and will be the subject of future work.

The objective of this work is to develop and verify a mathematical model that enables the prediction of residual stresses caused by heat treating cast aluminum alloy components. The model is based on the commercially available software ABAQUS. This software can perform all the required simulations provided that the necessary material properties are made available to it. These include thermal properties, such as the coefficient of thermal expansion, the specific heat, etc., and mechanical properties, such as the modulus of elasticity, the yield strength, etc., all as functions of temperature. Consequently, the first Task in the project focused on generating the necessary database. The database was obtained by calculations and measurements made on A356 alloy specimens using a modified Instron tensile testing machine. In addition, boundary conditions – in the form of heat transfer coefficients for each of the heat treatment steps - were obtained from measurements performed with a special quenching system. Once, this was accomplished, the second Task in the project commenced and focused on developing the model and using the software, database, and boundary conditions to predict the response of a commercial A356 cast component to a standard commercial heat treating cycle. In the third Task, the predicted responses were compared to experimentally measured responses.

2. Methodology

Selection of the Programming Code

Among the many finite element codes that are commercially available today, ABAQUS enables a wide range of linear and nonlinear engineering simulations to be performed efficiently, and therefore it is widely used. Because of its popularity and its ability to perform the required simulations accurately and efficiently, ABAQUS was selected for this project. It is a general purpose finite element code with the capability for sequentially coupled thermal and stress analysis to simulate solid material heat conduction/convection with general temperature-dependent conductivity, internal energy, and radiation boundary conditions. Moreover, ABAQUS has the special feature of allowing the user to prescribe user-defined material properties and analysis parameters that can vary with time and/or temperature. These user subroutines are written in the FORTRAN language and are compiled before the model is run. For example, in this work, this aspect of ABAQUS was used in the thermal analysis module to specify the direction and velocity of quenching and also in prescribing the quenching heat transfer coefficient as a function of temperature.

For predicting the response of the casting to quenching, ABAQUS performs two separate simulations in sequence. First, it performs a heat transfer analysis for quenching that produces the temperature profile in the part as it cools down from the solutionizing temperature. Next, it performs a mechanical simulation that calculates the evolution of stresses and the final distortion in the part. In each step, different initial conditions, boundary

conditions and material properties are used. The flow chart shown in Figure 1 illustrates the simulation procedure which involves the following simulation steps:

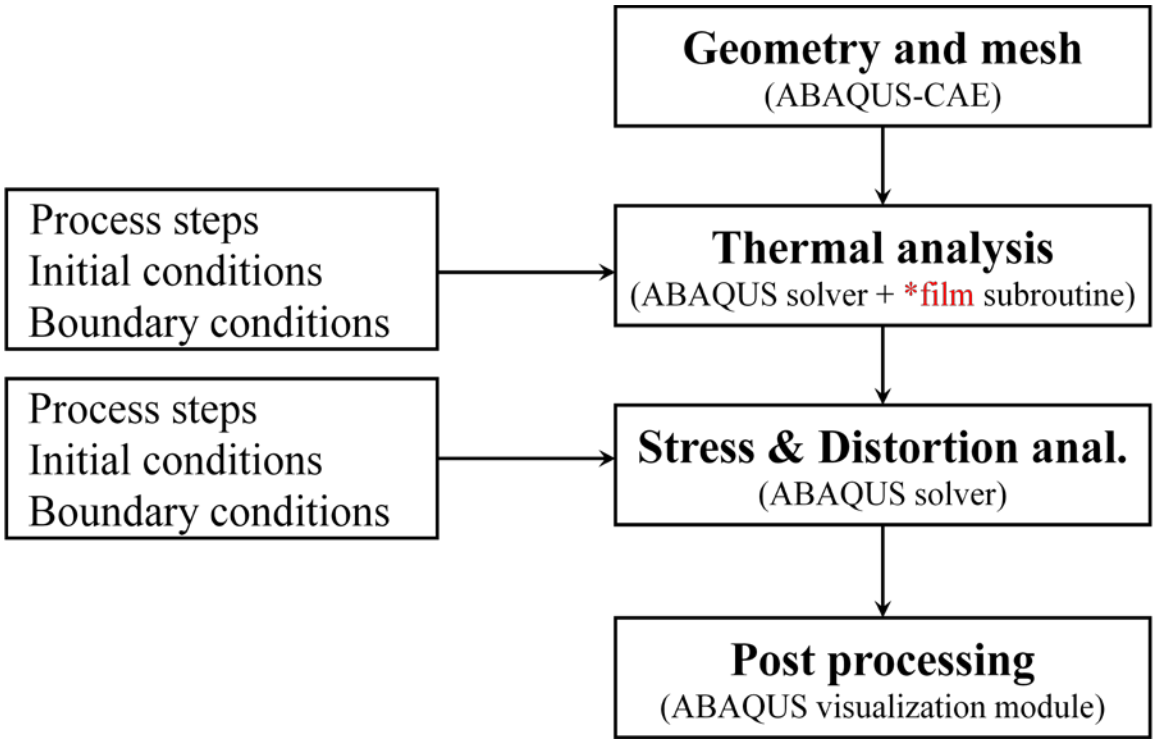

Figure 1. Solution procedures for the ABAQUS model.

1. Thermal Analysis Module

Heat transfer across the metal/fluid interface is a most significant aspect of the heat treatment processes because it controls the cooling rate which in turn determines the distribution and severity of residual stress created in the casting. The heat treatment process consists of

several steps, each of which imposes different boundary conditions on the model. Pre-heat treatment machining processes may induce residual stresses in castings. However, during solutionizing, these stresses are removed and it is assumed that the casting enters the quenching fluid in a stress-free condition.

Therefore, at time t=0, the casting is assumed to be at equilibrium at room temperature. It is then homogenized at an elevated temperature for a prescribed time. After homogenization, it is exposed to room temperature and then it is quenched. It is necessary to characterize the heat transfer coefficient from the surfaces of the casting to the environment during these steps.

During the process of dipping the casting into the quenching medium, the casting becomes partially covered with the fluid, and as the casting moves deeper into the fluid, more of its surface becomes covered with the fluid. Regions on the casting's surface that are in the fluid lose heat at a different rate than regions that are in the air.

Accordingly, the heat transfer coefficient must be varied on the surface of the part as it is continuously submerged into the fluid. The rate of heat loss due to convection q_c is determined from Eq. (1):

$$q_c = h_c(T - T_\infty)^a(T - T_\infty) \quad \text{where} \quad h_c = h_w \qquad h_c = h_a \tag{1}$$

In Eq. (1), h_w and h_a are the convective heat transfer coefficients from the casting surface to water, and from the casting surface to air, respectively. T is the surface temperature, and T_∞ is the ambient temperature. The exponent, a, has a value of zero for forced convection (in our case), and a value of 0.25 for free convection.

2. Stress Analysis Module

In the thermal analysis module, the temperature is the unknown variable. In the stress analysis module, the displacement and stress are the unknown variables. The thermal fields affect the mechanical fields through thermal expansion and temperature-dependent material properties. The relationship is given by Eq. (2).

$$\varepsilon^{th} = \alpha(\theta)(\theta - \theta^0) - \alpha(\theta^I)(\theta^I - \theta^0) \tag{2}$$

In Eq. (2), $\alpha(\theta)$ is the coefficient of thermal expansion, θ is the current temperature, θ^I is the initial temperature and θ^0 is the reference temperature for the expansion coefficient. At this temperature the thermal expansion is assumed to be zero [5].

In order to perform stress analysis based on the transient temperature distribution predicted by the thermal module it assumed that all the residual stresses that were introduced into the casting during its manufacturing have been removed during solutionizing. An elastic-plastic analysis is therefore performed in order to account for material yielding as the casting is cooled from high solutionizing temperature where the mechanical properties of the alloy are severely diminished.

The stress analysis module uses the same time increment that is used in the thermal module, but if desired, the time increment can be refined to enhance the accuracy of the stress analysis.

3. Materials and Procedures

Materials

Aluminum casting alloy A356.2 with the chemical composition shown in Table 1 was used to develop and demonstrate the procedure for obtaining the necessary database and modeling the response of aluminum alloy cast components to heat treatment. Because it is heat treatable and precipitate hardenable, and because it has excellent castability, good corrosion resistance and good machinability, this alloy is used extensively in many applications including military and aerospace applications.

Table 1: Composition of A356.2

Si	Fe	Cu	Ti	Mg	Others
7.25	0.08	0.005	0.27	0.27	< 0.002

Procedures

Aluminum A356.2 standard tensile bars similar to that shown in Figure 2 were cast in a steel mold. The mold was preheated to 427°C (800°F) in a GECO BHT30 furnace. About 40 lbs of A356.2 ingot were melted in a MELLEN CC12 resistance furnace and cast into the pre-heated steel mold. A 0.2%wt of TiB (5Ti: 1B) grain refiner was added to the melt. Prior to casting, the melt was degassed for about 40 minutes with a rotary impeller and Argon gas

[6, 7]. While degassing, the melt temperature was maintained at 750°C (1382°F). The melt was poured at 800°C (1472°F).

Microstructures of as-cast and solutionized specimens taken from the tensile bars are shown in Figure 3Figure 4, respectively. For the solutionized condition, specimens were held at 538°C (1000°F) and then rapidly quenched in room temperature water. The Si particles were spheroidized and coarsened after this homogenization treatment.

Figure 2. Cast A356.2 standard tensile bar.

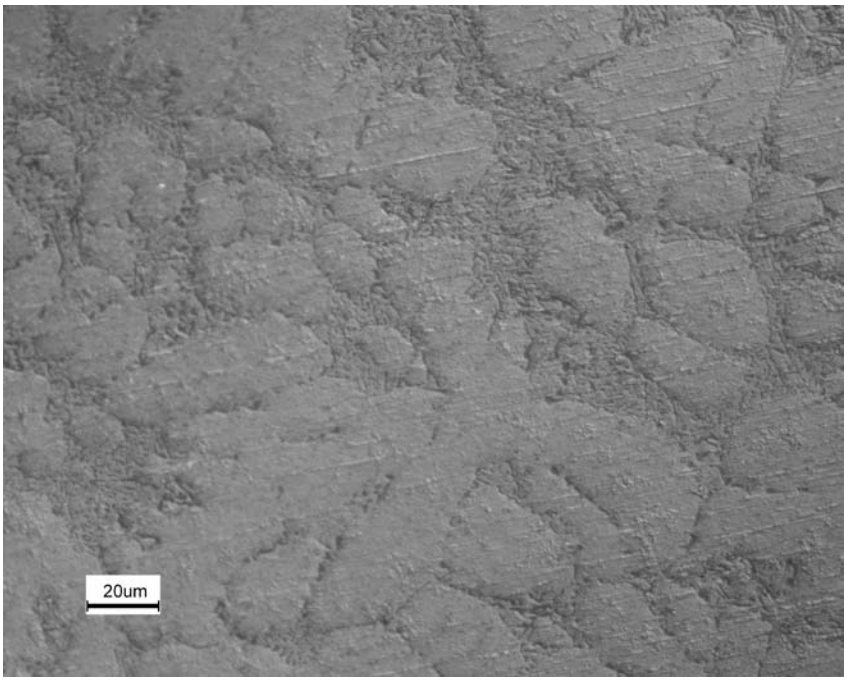

Figure 3. Microstructure of as-cast A356 alloy.

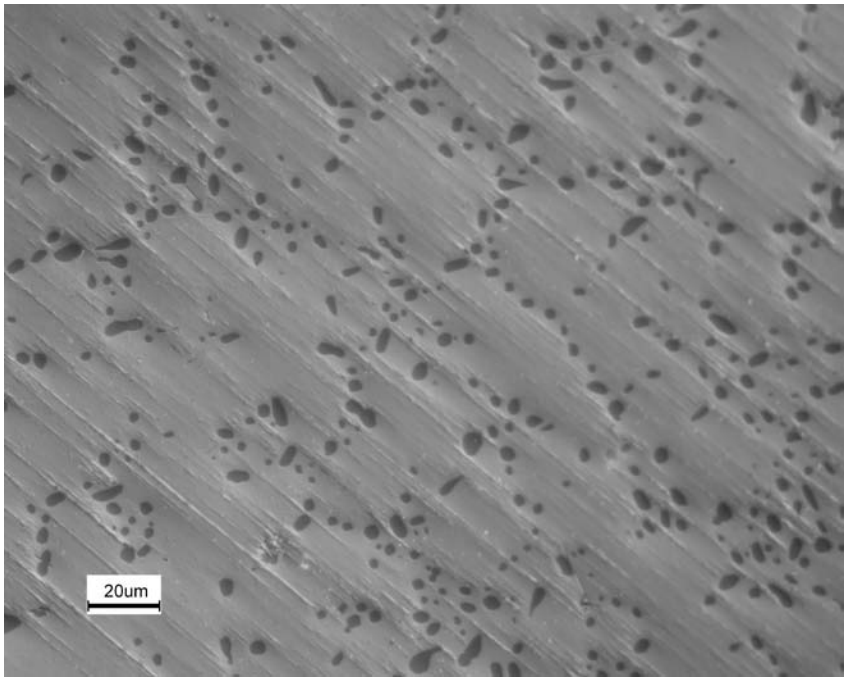

Figure 4. Microstructure of solutionized A356 alloy.

Generation of Physical Properties

The necessary database for ABAQUS contains the density specific heat and thermal conductivity of the alloy. These properties can be generated by JMatPro software[2], which is a powerful software that calculates properties of multi component alloys. The data used in this work is shown in Table 2. Data generated by JMatPro Software.

Table 2. Data generated by JMatPro Software.

Property	Temperature: 25°C – 538°C (Linear)
Specific Heat (T)	886 – 1300 ($J.Kg^{-1}°C^{-1}$)
Density (T)	2674 – 2576 ($Kg.m^{-3}$)
Expansion Coefficient (T)	21.13 – 26.2 (10^{-6} $°C^{-1}$)
Poisson's Ratio (T)	0.330 – 0.359

Thermal conductivity at elevated temperature was calculated from electrical resistivity measurements and the Wiedemann-Franz law which states that the ratio of electronic contribution to thermal conductivity (k) of a metal is proportional to temperature as shown in Eq. (3). The calculated thermal conductivity as a function of temperature is shown in Figure 5.

[2]JMat Pro is marketed by Thermotech Sente Software.

$$\frac{k}{\sigma} = LT \tag{3}$$

$$L = \frac{k}{\sigma T} = \frac{\pi^2}{3}\left(\frac{k_B}{e}\right)^2 = 2.44 \times 10^{-8} W\Omega K^{-2} \tag{4}$$

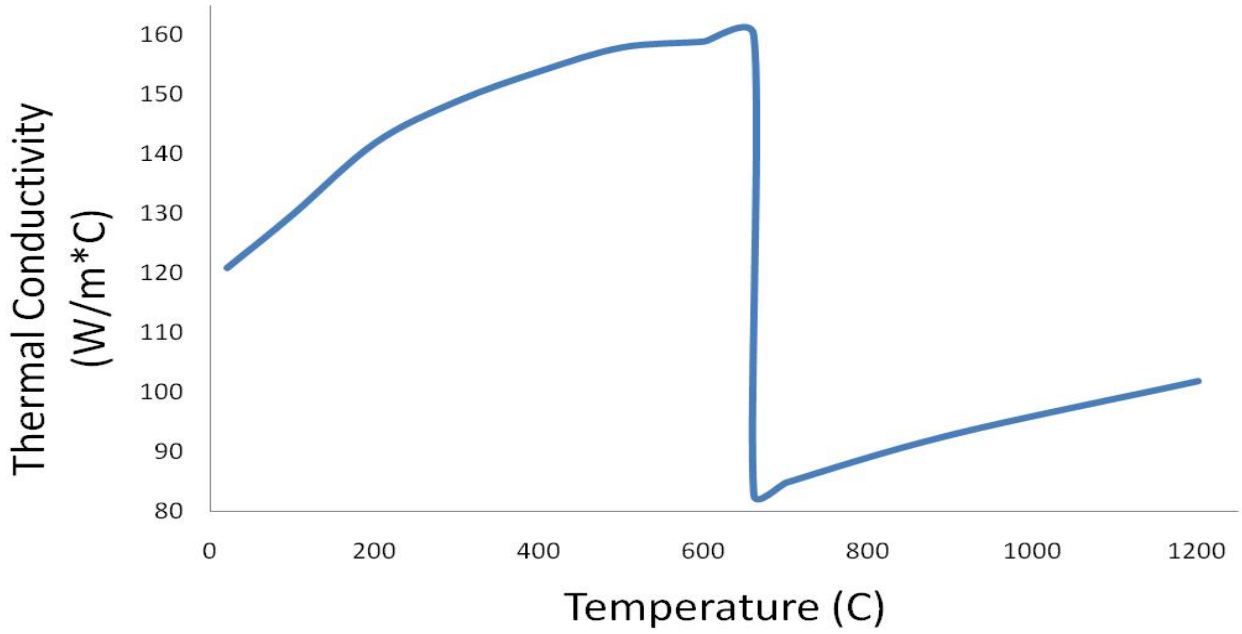

Figure 5. Calculated thermal conductivity as a function of temperature.

Measurement of the Quenching Heat Transfer Coefficient

The quenching heat transfer coefficient is used by the thermal module in ABAQUS to compute the heat that is transferred out of the part during quenching. The heat transfer coefficient is measured with the apparatus shown in Figure 6 [8]. The measurement involves quenching a heated cylindrical probe that is machined from a cast piece of A356.2 alloy and

equipped with a thermocouple connected to a fast data acquisition system into the quenching medium and acquiring the temperature-time profile. The probe dimensions are chosen such that the Biot number for the quenching process is <0.1. This insures that significant thermal gradients will not be present in the radial direction in the probe. Accordingly, a simple heat balance analysis (usually referred to as a lumped parameter analysis) can be performed on the system (probe + quenching medium) to yield the heat transfer coefficient. Since the Bi < 0.1, the error associated with the calculation of the heat transfer coefficient is less than 5%. For this work, a small cylindrical probe with dimension of 0.374" (9.5 mm) in diameter and 1.496" (38mm) long shown schematically in Figure 7, was cast from a standard A356.2 alloy. A hole was drilled down to the geometrical center of this probe and a thermocouple was inserted for measuring the time-temperature data. Graphite powder was packed into the hole before the thermocouple was inserted in order to ensure intimate contact between the probe and the thermocouple. The probe was heated to the solutionizing temperature and held at that temperature for 12 hours in order to ensure homogenization. Subsequently, the probe was quenched in water that was maintained at room temperature. While quenching, the temperature of the probe was acquired as a function of time using a fast data acquisition system at a scan rate of 1000 scans/sec. A quench tank with two liters of water was used and the probe was immersed completely in the water. The temperature of the water before and after quenching remained constant at 17°C (63°F). A heat balance applied to the probe results in Eq. (5), which was used to calculate the heat transfer coefficient at the surface of the probe.

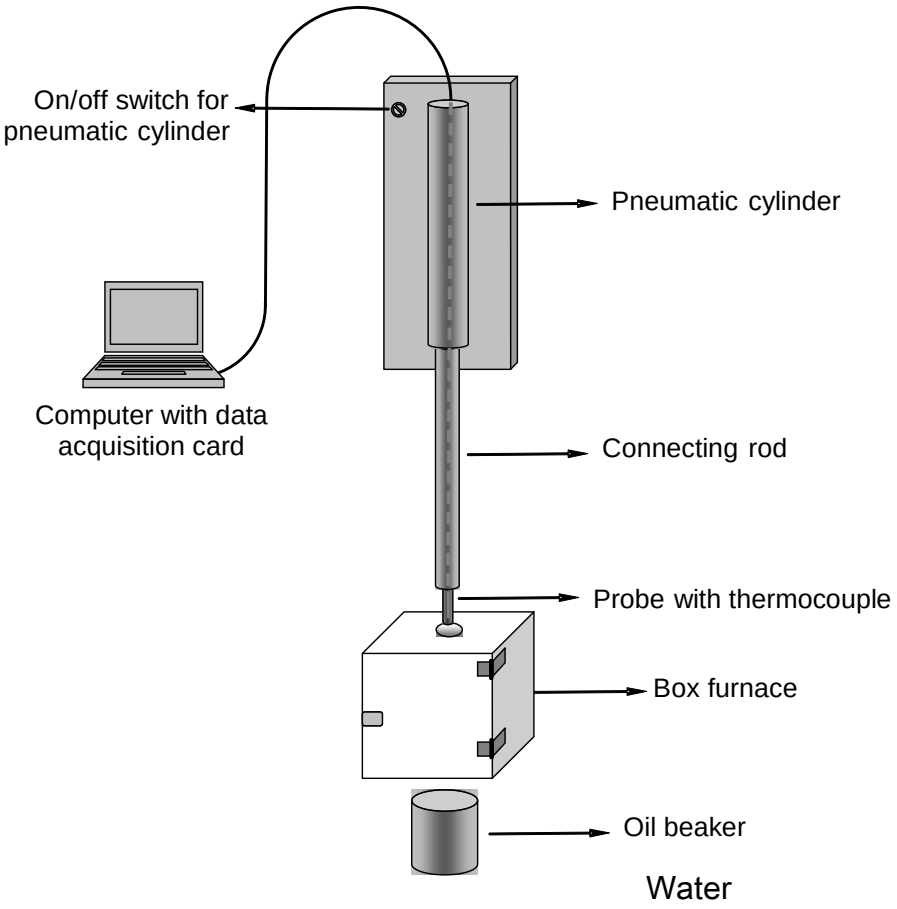

Figure 6. Quenching probe system.

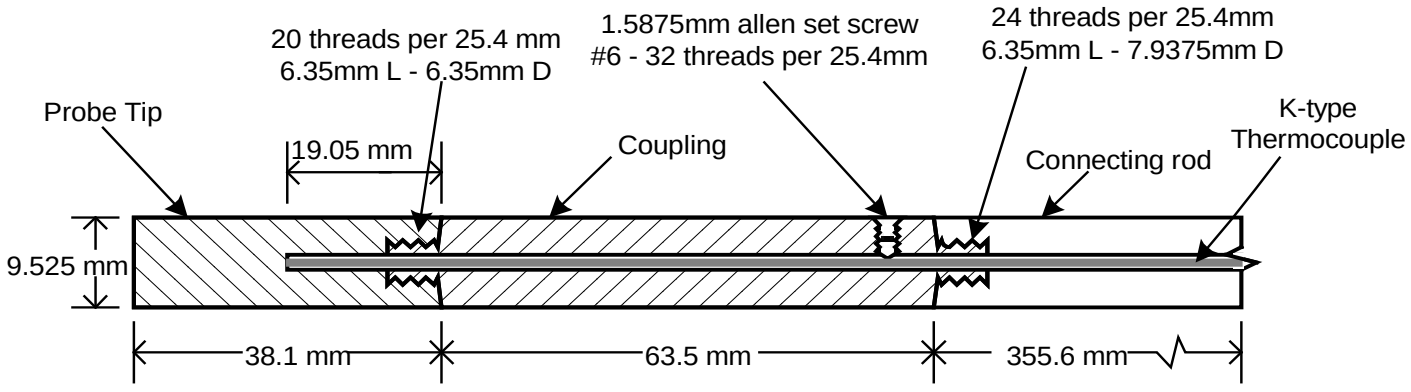

Figure 7.Quench probe-coupling-connecting rod assembly.

$$h = -\frac{\rho V C_p}{A_s\left(T_s - T_f\right)}\frac{dT}{dt} \tag{5}$$

In Eq. (5), h is the heat transfer coefficient at the surface of the probe, ρ, V, C_p and A_s are the density, volume, specific heat, and surface area of the probe, respectively. T_s is the temperature at the surface of the probe, which, due to the geometry of the probe, is approximately equal to the measured temperature at the center of the probe. T_f is the bulk temperature of the quenching medium. The derivative of temperature with respect to time in Eq. (5) is calculated from the measured temperature vs. time data.

The quenching heat transfer coefficient was measured for quenching at 2 different velocities, namely 1,000 and 1,200 mm/s. The maximum heat transfer coefficient was found to shift to lower temperature as the quenching velocity increased. The reason for this behavior is not clear. The measured cooling curves are shown in Figure 8, and the calculated cooling rate vs. temperature at different quench velocities are shown in Figure 9. The quenching heat transfer coefficients for the different quenching velocities are shown in Figure 10.

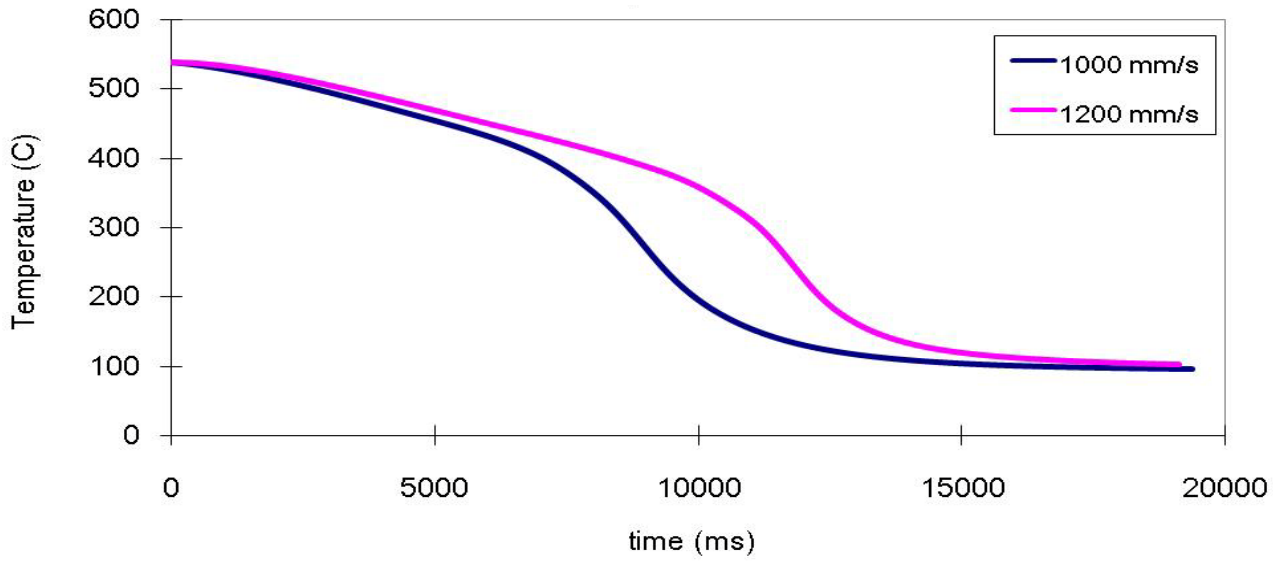

Figure 8. Measured cooling curves for A 356 alloy.

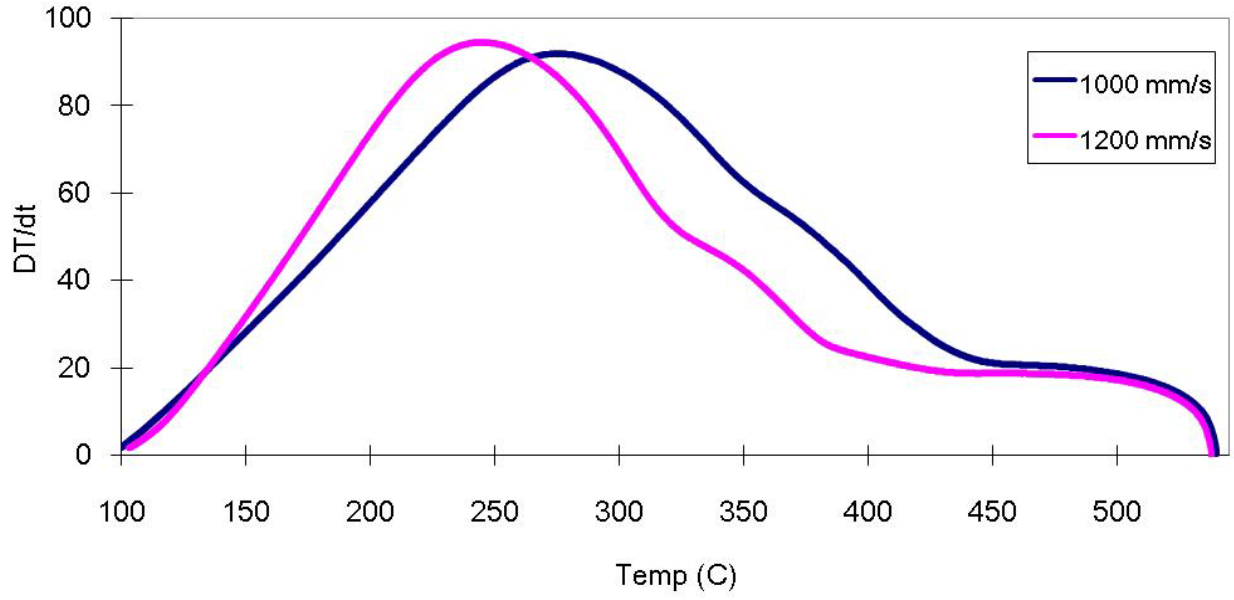

Figure 9. Calculated cooling rate vs. temperature for A356 alloy.

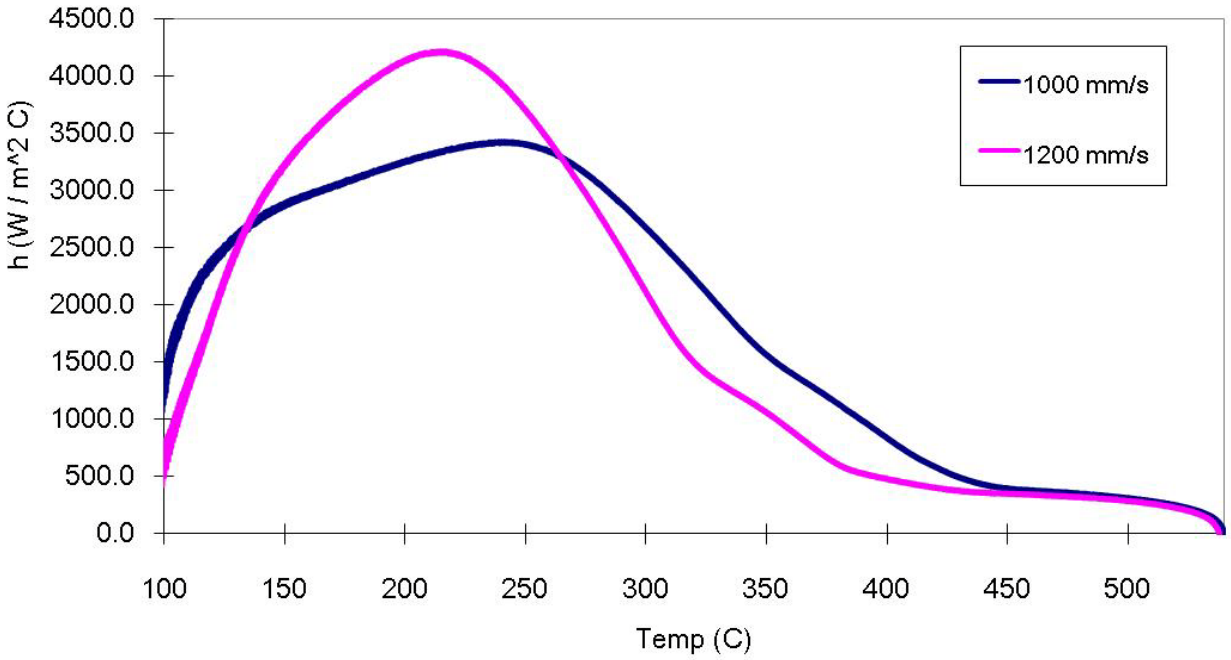

Figure 10. Calculated quenching heat transfer coefficient curves for A356 alloy.

Measurement of Surface Roughness

In order to guarantee a similar surface micro-profile for the quenching probe and the modeled component, surface roughness measurements were performed on the quenching probes and the part to be modeled. Measurements were made with a UBM Laser Microscope[3] and the results are shown in Figure 11 and 12. Surface roughness measurements show that the superficial roughness is 0.501 μm Sa (mean superficial micro-profile amplitude) for the part and 0.398 μm Sa for the quenching probe. Muojekwu, et al. [9] have shown that such difference in surface roughness has negligible effect on the magnitude of the quenching heat transfer coefficient.

[3] Received from Solarius Development Inc.

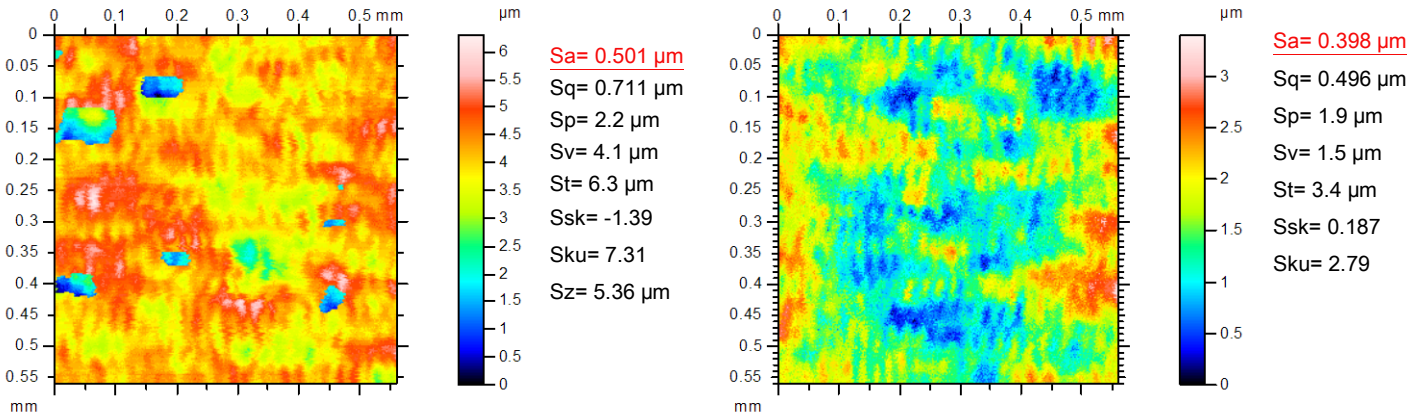

(a) (b)

Figure 11.Measured surface roughness for (a) the cast part, and (b) the probe.

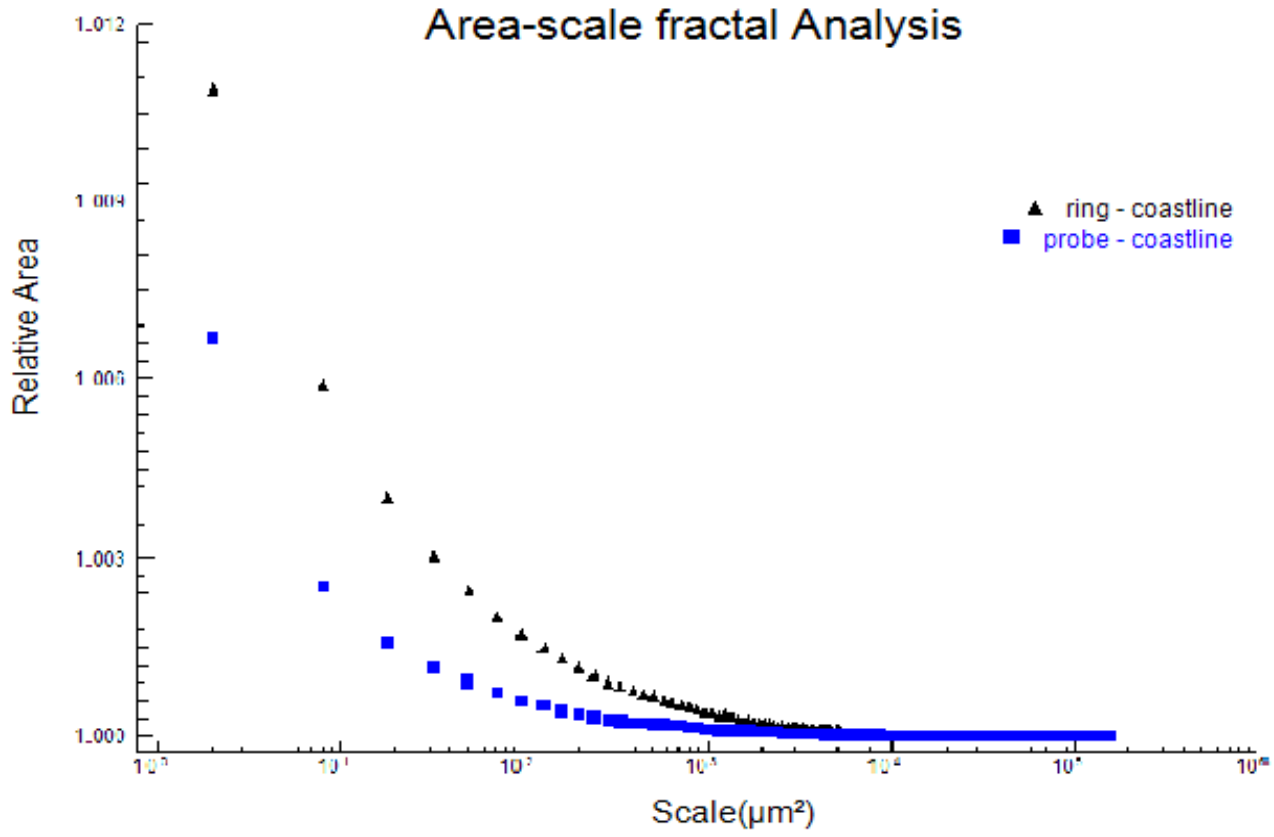

Figure 12. Surface roughness comparison for A 356 alloy.

Generation of Mechanical Properties

The required mechanical properties are the Young's modulus, Poisson's ratio and the stress-strain curve (including working hardening) over the entire heat treatment temperature range. Stress-strain curves are obtained by measurements. This information is needed by the stress analysis module to compute the stresses that develop in the part during heat treatment.

The thermal-stress and distortion develop in the first few seconds after quenching, while the material is still a supersaturated solid solution, and before any precipitation has occurred. Therefore, the properties of the supersaturated solid solution must be used. In order to demonstrate the difference between the mechanical properties of the supersaturated solid solution and the equilibrium casting, the following were used in tensile tests: (1) Specimens that were solutionized at 538°C (1000°F) and then rapidly quenched in room temperature water, and (2) Specimens that were solutionized at 538°C (1000°F) and then furnace-cooled to room temperature.

An Instron universal testing machine[4] was used for measuring the room temperature mechanical properties. The elastic modulus, yield stress, and plastic strain of the alloy were calculated from these measurements. Sufficient measurements were made in order to obtain accurate representation of these properties. The resulting room temperature stress-strain curves under several strain rates are shown in Figure 13. Water quenched tensile bars show higher ultimate tensile stress and yield stress, and lower Elastic modulus. The Figure shows that the yield strength of this alloy increases as the strain rate decreases.

[4] Instron Worldwide Headquarters, 825 University Ave, Norwood, MA 02062-2643, USA

The mechanical properties of A356 alloy at elevated temperature were obtained from Maijer, et al. [10]. These measurements were performed on samples that were previously heated and quenched. The samples were re-heated in a Gleeble to 540°C (1004°F) for 30 seconds in order to create a supersaturated solid solution, and then they were cooled at a rate of 5°C /s by water cooled platens. Measurements were performed when the desired temperature was attained. The stress-strain curves are shown in Figure 14. The Figure shows that above 300°C (572°F), the strength increases as the strain rate increases. However, below 300°C (572°F), the opposite is true and the strength decreases as the strain rate increases. This may be because Mg-Si particles form in this temperature range and affect the strength of the alloy. [11, 12]

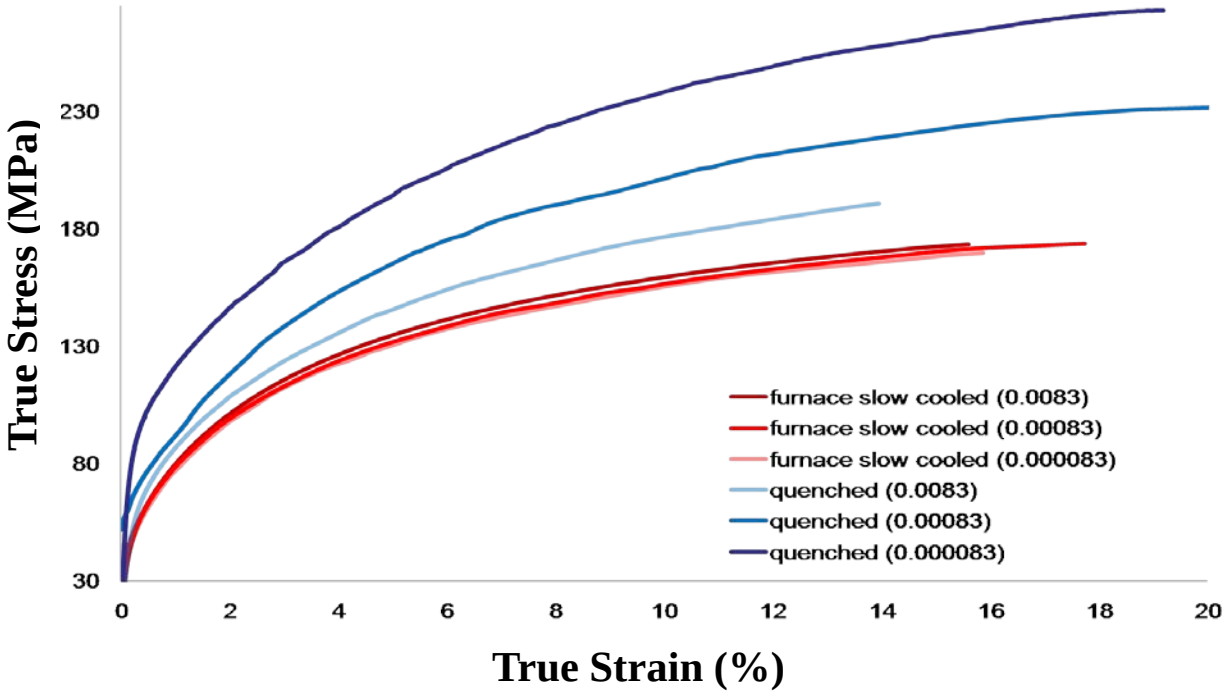

Figure 13. True stress-strain curves for water-quenched and slow-cooled samples at strain rates = 0.0083/s, 0.00083/s and 0.000083/s.

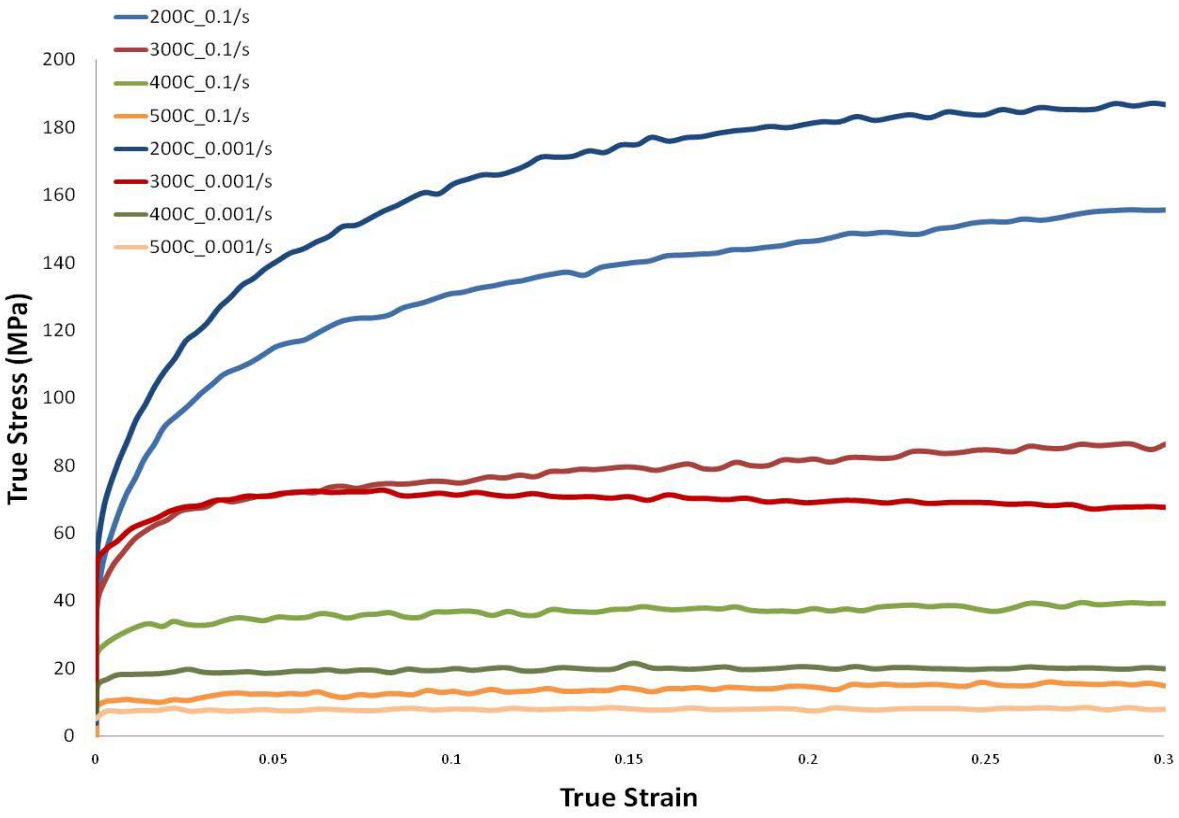

Figure 14. True stress-strain curves for supersaturated alloy at elevated temperature for strain rates = 0.001/s and 0.1/s. [10]

4. Model Construction

The Modeled Part

The part shown in Figure 15 was chosen to demonstrate the model and verify the accuracy of its prediction. This design contains both thick and thin wall sections, and its symmetrical shape reduces both quenching and measuring difficulties. The distortion and residual stresses are expected to be concentrated in the thin wall section.

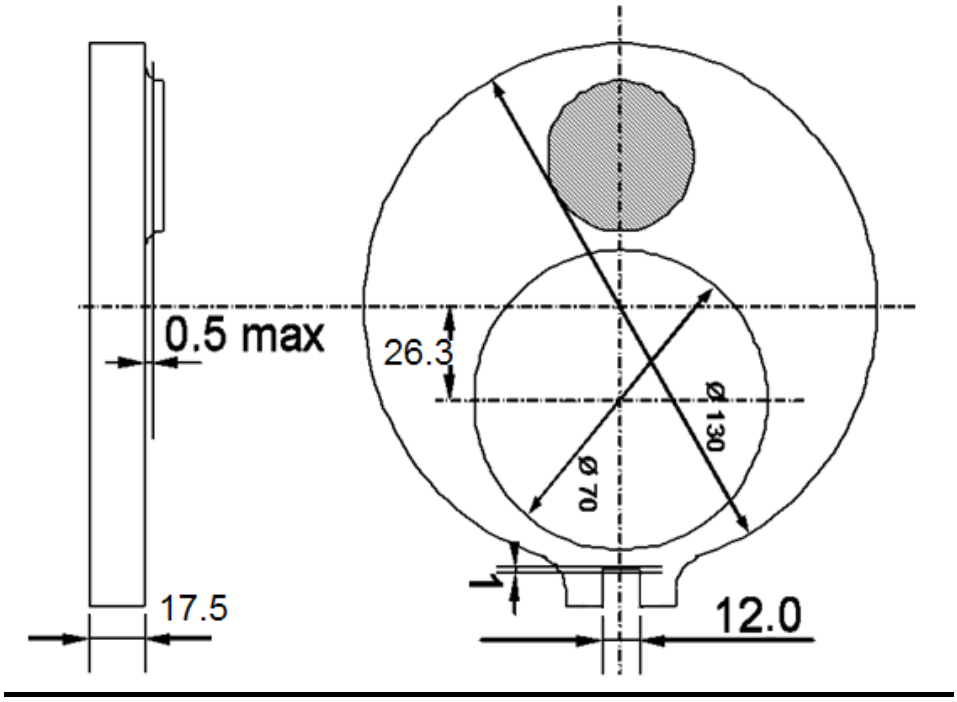

Figure 15: The modeled part[5].

[5] Courtesy of Montupet S.A., 60180 Nogent Sur Oise, France.

Mesh Development

The part geometry shown in Figure 15 was meshed by the ABAQUS pre-processor. Three different mesh sizes were used: large, medium, and small. All three meshes were generated with built-in curvature control and a deviation factor as shown in Figure 16, 17 and 18. The sensitivity of the simulation to the nodal spacing is an important aspect of any numerical simulation and the results of the finite element simulation will depend on the design of the mesh. In general, as the spacing between nodes is made smaller, the solution becomes more accurate. However, this increase in accuracy will be accompanied by a substantial increase in computing time. Therefore, the mesh must to be small enough to produce reasonable values for the force and displacement, but large enough to perform the calculation in acceptable time. The heat transfer module was used to assess the effect of mesh density on model predictions. Specifically, quenching the part vertically with a velocity of 1000 mm/s was modeled using the three mesh sizes.

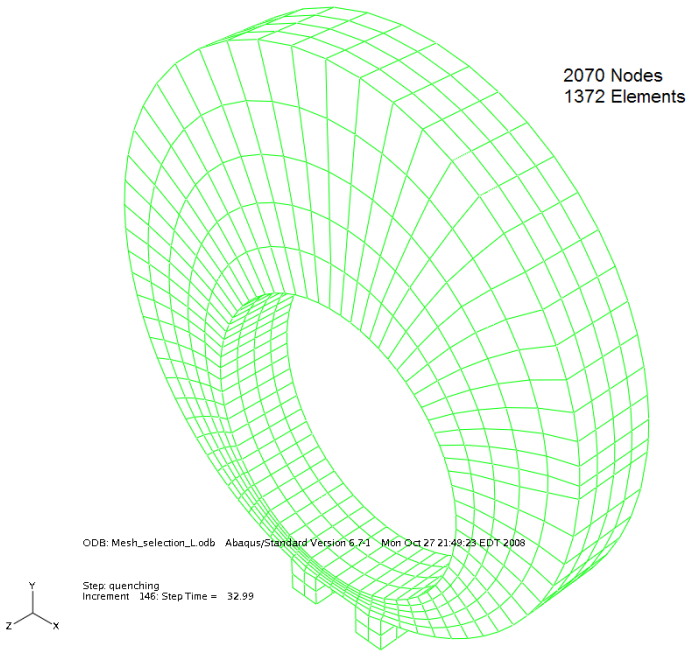

Figure 16. Large mesh.

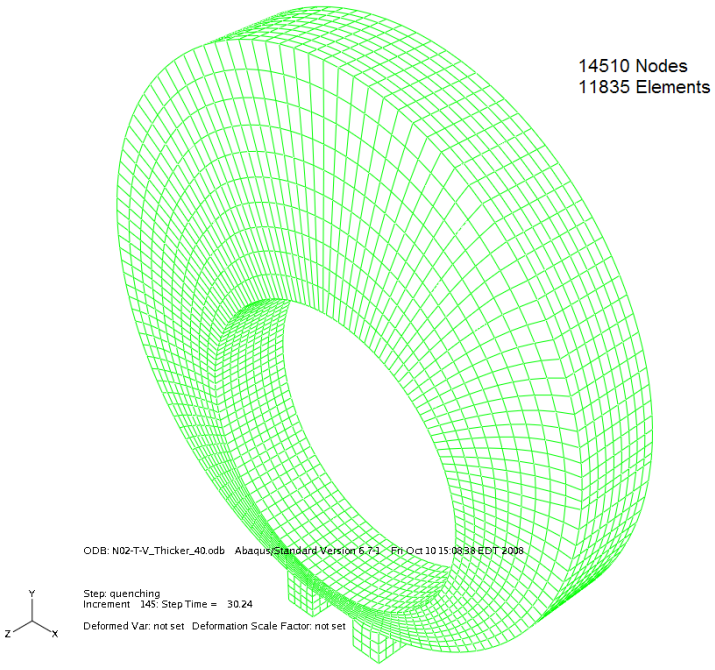

Figure 17. Medium mesh.

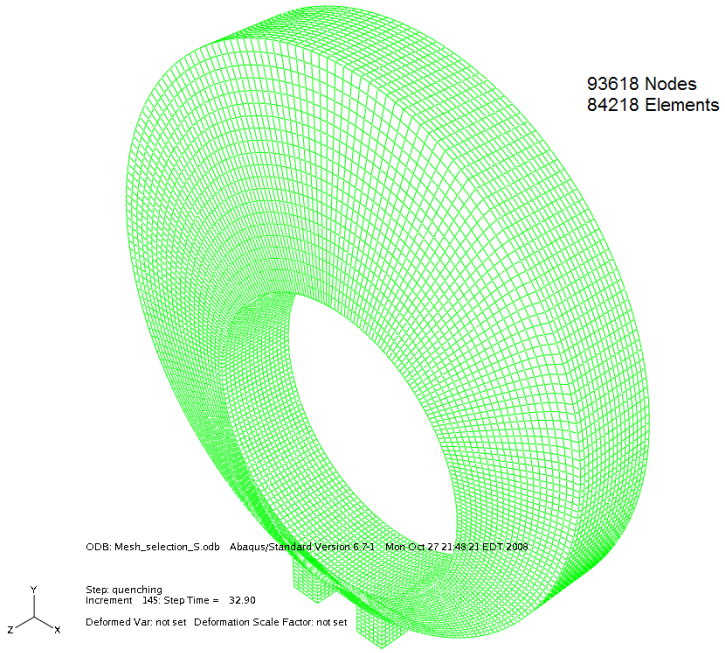

Figure 18. Small mesh

The results are shown for the node marked in red in Figure 19 because this node is the most sensitive node to mesh refinement since it is located in the thickest section of the part. The model-predicted cooling curves at this point are presented in Figure 20 and the cooling rates during quenching are shown in Figure 21. The maximum temperature at the highest cooling rate as predicted by the large mesh is 271.4℃(520°F), the medium mesh predicted 291.9℃ (557°F) and the small mesh predicted 295.5℃ (564°F). The difference in maximum cooling rate as predicted by the small and large meshes is 1.76% and the difference in maximum cooling rate as predicted by the small and medium meshes is less than 0.289 %. Figure 22 shows the computing time for the three simulations. It is believed that the medium mesh provides a good balance between prediction accuracy and computing time. With the medium mesh the geometry contains 11,835 hexahedral elements and 14,510 nodes.

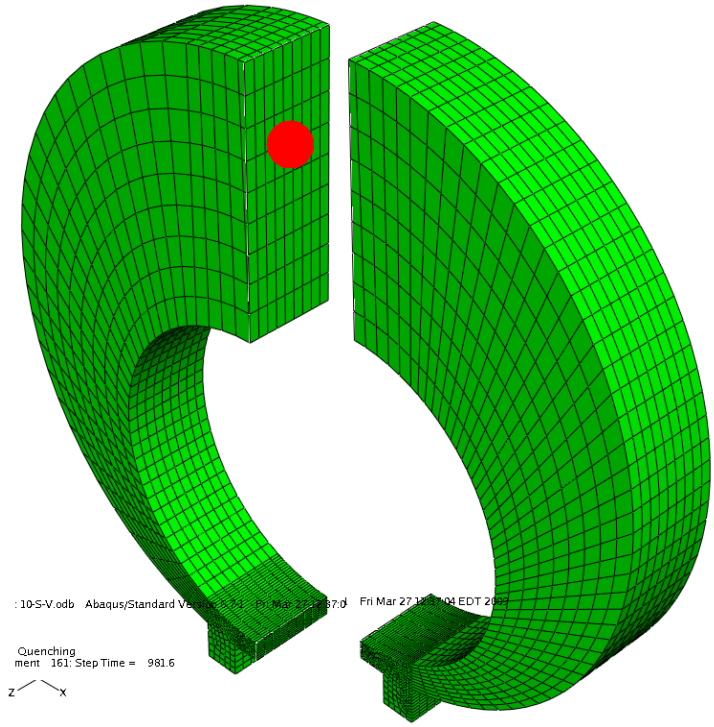

Figure 19. Location of node selected for mesh development.

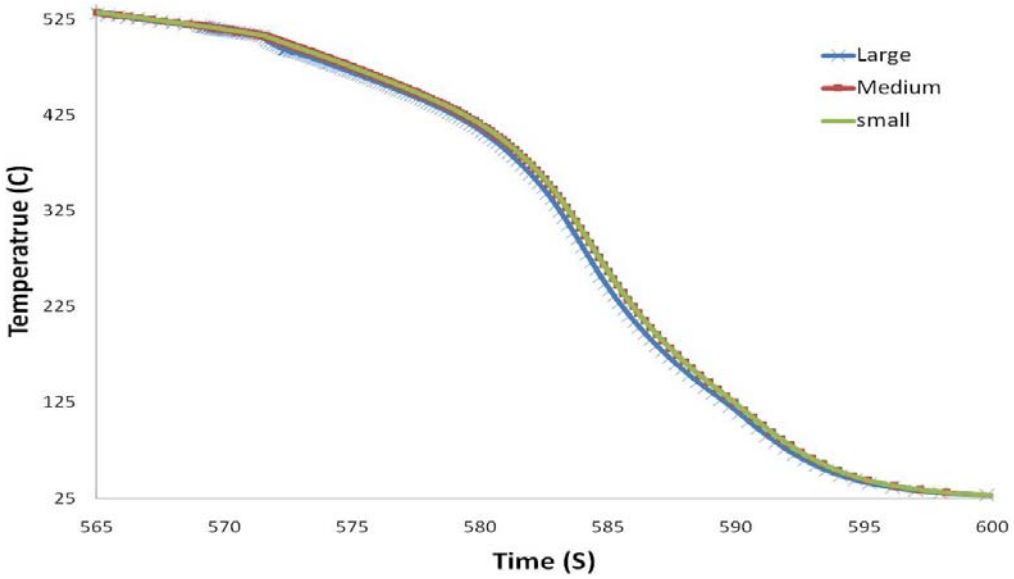

Figure 20. Cooling curves at the selected point obtained by simulation with different mesh densities.

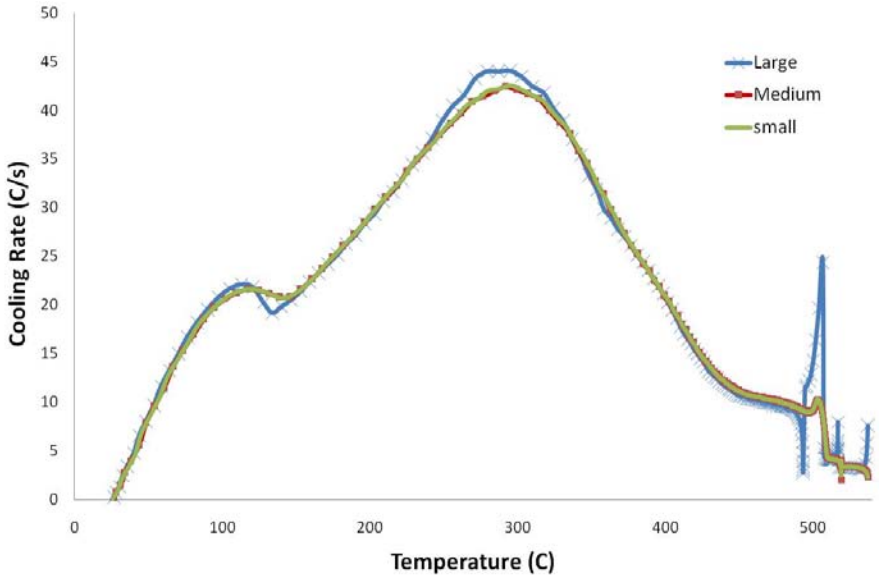

Figure 21. Cooling rates at the selected node obtained by simulation with different mesh densities.

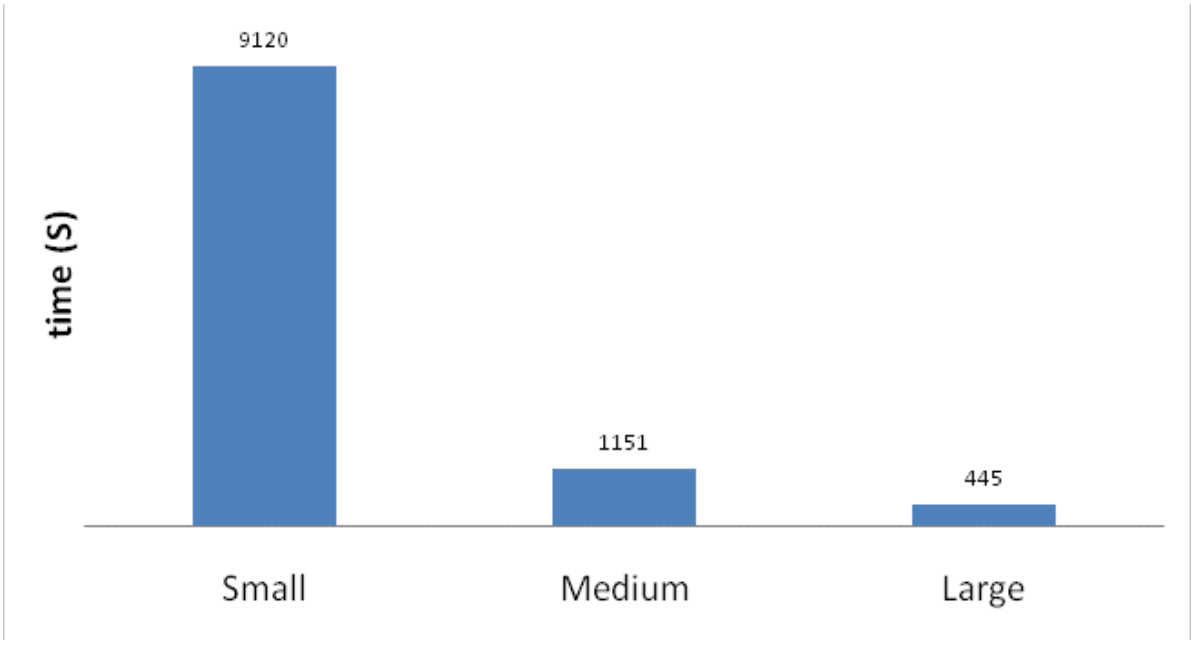

Figure 22. Computational time for the different mesh densities.

Because the thinner sections of the geometry are more sensitive than the thicker sections to temperature and stress, the graded mesh geometry, which is shown in Figure 23 and is based on the medium mesh, was used. In this mesh design, the mesh density is increased in the thin sections of the geometry. The DC3D8 element is used in the heat transfer simulation. This is an eight-node continuum-diffusive linear three dimensional brick element. On the other hand, the C3D8R element is used in the stress module. This is an eight-node linear reduced integration three dimensional brick continuum element with hourglass control.

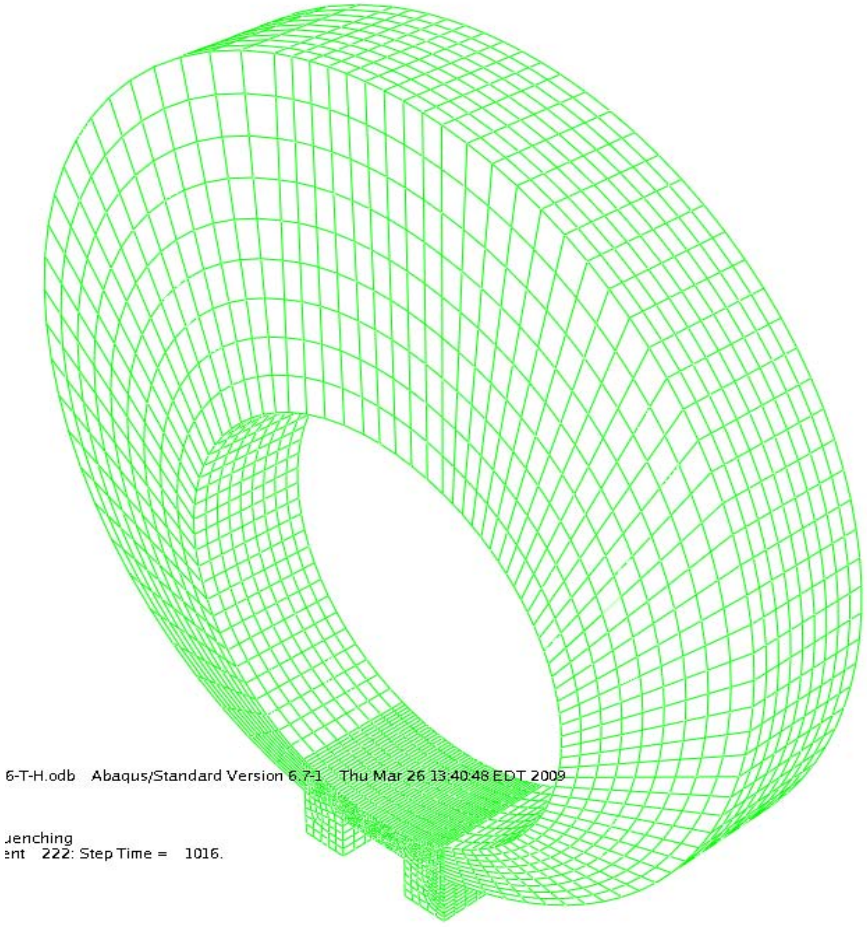

Figure 23. Refined mesh.

5. Computer Simulations

The Thermal Module

As shown schematically in Figure 24, two heat transfer simulations were performed on the meshed geometry. In the first simulation, the part is vertically quenched into the water tank. In the second simulation, the part is horizontally quenched into the water tank.

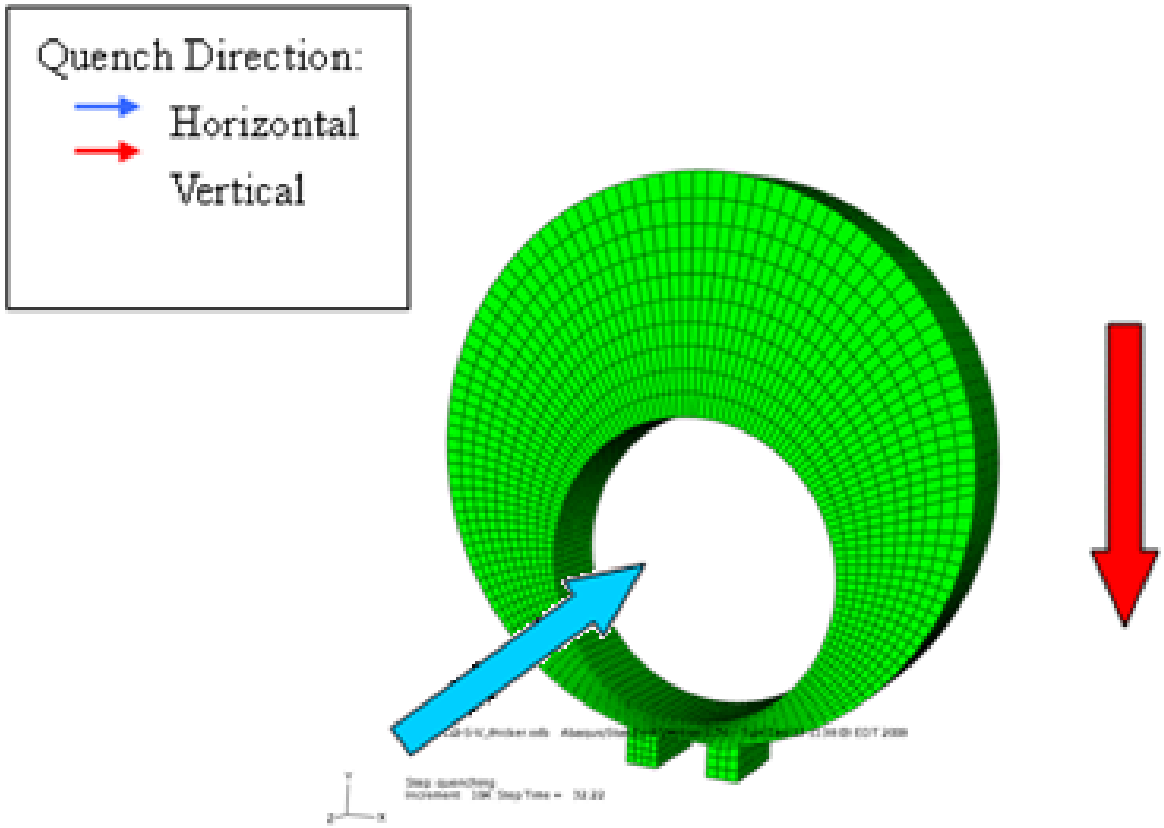

Figure 24. Schematic representation of the directions in which the parts were quenched.

The following sequence was used to model the heat treatment of the part: Furnace heating to 538°C (1000°F), followed by a dwell in room temperature air for 6 seconds, followed by immersion into the quench tank with a velocity of 1000 mm/s, followed by quenching in water to room temperature. The initial conditions used for the thermal module included the temperature of the part before heat-treating (room temperature in this case), and the mode of heat treatment. The boundary conditions used to represent each of the steps of the heat treatment process were as follows:

- For the furnace-heating step: A convective boundary condition was used at all surfaces of the part by providing the rough heat transfer coefficient (50 W/m^2)for heating the part in the furnace up to the homogenization temperature of 538°C (1000°F).

- For the dwell step: A convective boundary condition was used at all surfaces of the part by providing the air heat transfer coefficient (200 W/m^2). The ambient temperature was room temperature.

- For the immersion step: The direction and velocity of immersing the part into the quench tank were defined. This step is important in order to capture the temperature gradient along the immersion length of the part. In this demonstration, the part was immersed along (1) its length and (2) its thickness with a velocity of 1000 mm/s, and the process time for this step was 0.128 second for the vertical quenching and 0.018 second for the horizontal quenching. A convective boundary condition at all surfaces of the part was used by providing either the measured heat transfer coefficient for quenching the part in water or air heat transfer coefficient, depending on node location at processing time. This feature was specified via a user-developed subroutine.

– For the quenching step: A convective boundary condition at all surfaces of the part was used also by providing the measured heat transfer coefficient for quenching the part in water from the inherited temperature down to room temperature.

Vertical Immersion – In this simulation, the time for complete immersion is 0.128 s and this time span resulted in a maximum temperature difference of 18.7°C (65.7°F) between the bottom surface of the part (the surface that contacted the water first) and the top surface of the part (the surface that contacted the water last). The resulting temperature distribution is shown in Figure 25.

Horizontal Immersion – In this simulation, the time for complete immersion is 0.018542 s and this time span resulted in a maximum temperature difference of 16°C (60.8°F) between the bottom surface of the part and the top surface of the part. This is a more uniform temperature distribution, compared to the other quenching direction. The resulting temperature distribution is shown in Figure 26.

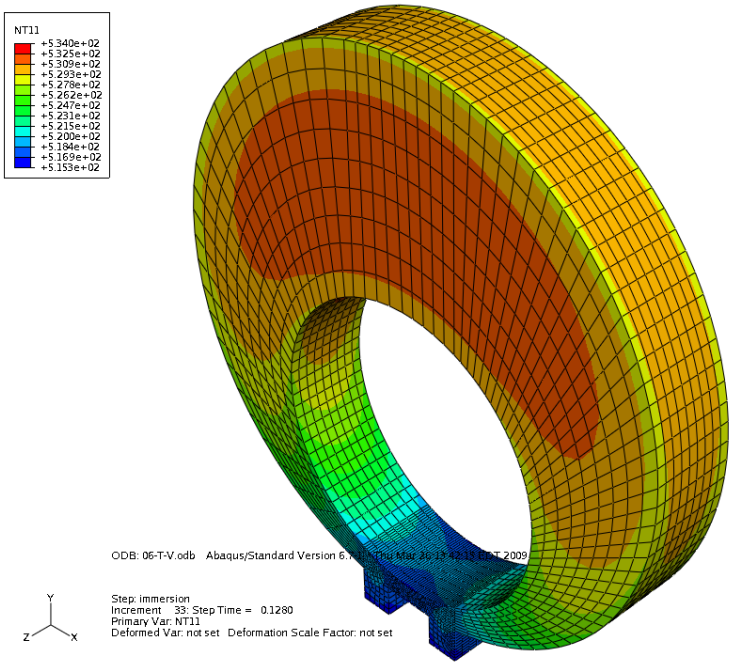

Figure 25. Thermal prediction for vertical quenching after immersion step.

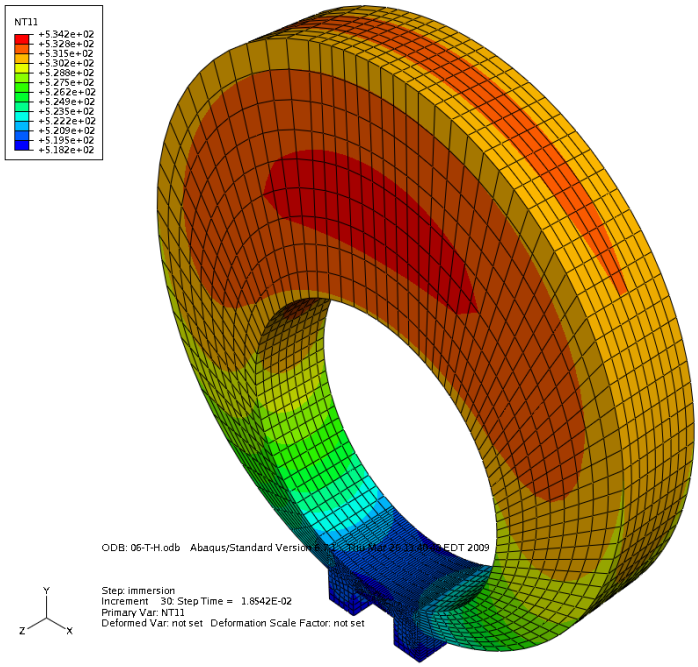

Figure 26. Thermal prediction for horizontal quenching after immersion step.

The Stress Module

The stress module calculates the residual stresses and distortion cause by the quench process. The analysis begins with the part in a stress-free state. However, if a known initial stress state existed, the appropriate values could be used. The deformation and stress developed in the casting during quenching depends on the rate of quenching. Therefore, the transient temperature history at each node during heat treatment is obtained from the heat transfer analysis. The finite element mesh and time increment which are used in the thermal module must be used in the stress module.

Nodal constraints are required in order to prevent rigid body displacement and rotation. This requirement applies to all the process steps, and is defined in the model input file. Referring to the 3-D geometry, 3 nodes at the center of the top face were constrained from moving. The quench-induced deformation and the quench-induced residual stress for both quenching directions are shown in Figure 27 and 29, respectively. For better visualization, the distortion results are shown magnified in Figure 28 and 30.

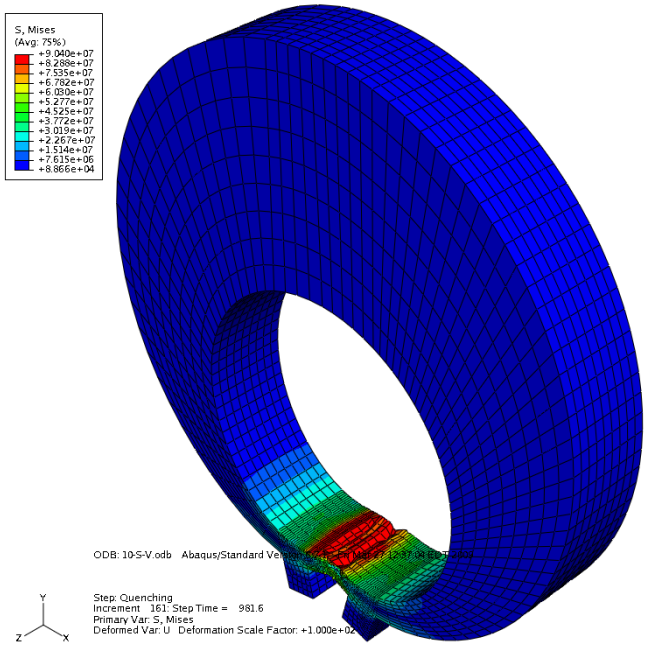

Figure 27. Thermal-stress prediction for vertical quenching after quenching step.

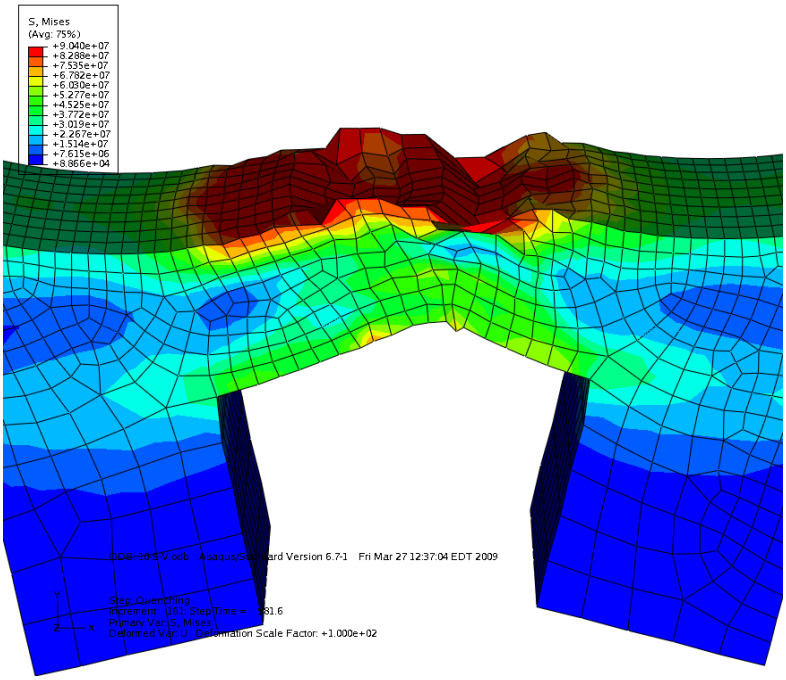

Figure 28. Thermal-stress prediction for vertical quenching after quenching step.

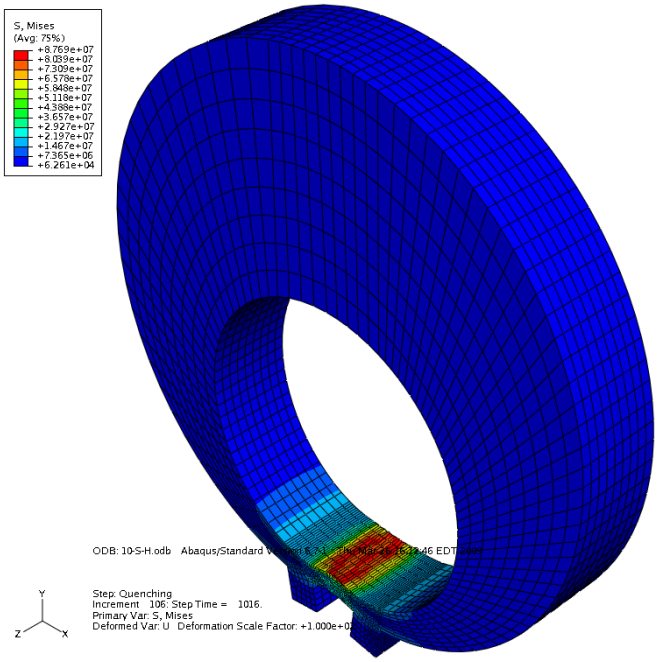

Figure 29. Thermal-stress prediction for horizontal quenching after quenching step.

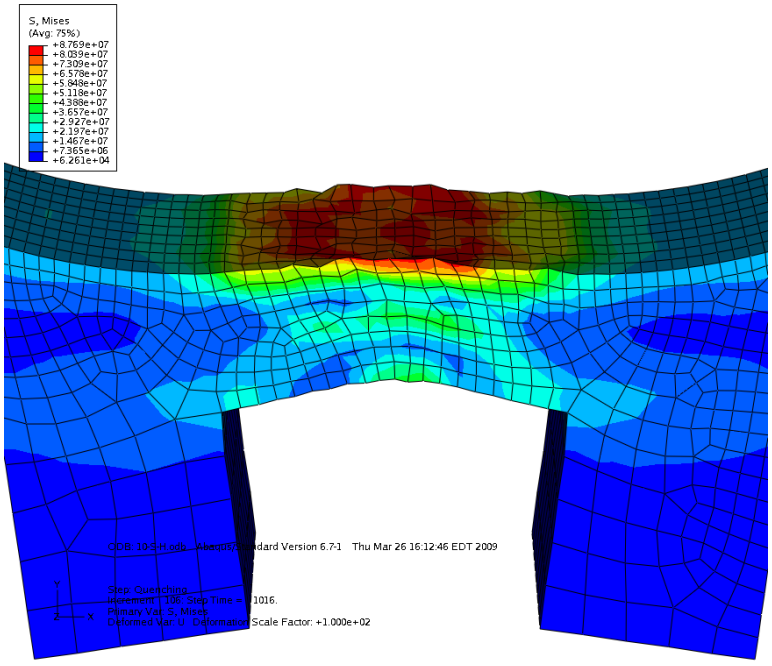

Figure 30. Thermal-stress prediction for horizontal quenching after quenching step.

5. Verification of the Model Predictions

The model predictions were verified by comparing them to measurements of corresponding parameters for parts made using processing conditions similar to those used in the simulation. The capabilities of the model are demonstrated using the part shown in Figure 31[6]. The castings were heat treated following the same procedure used in the simulation. Several repetitions were made for both vertical quenching and horizontal quenching in order ensure that the measurements are statistically valid.

Figure 31. Picture of the cast part.

[6] Courtesy of Montupet S.A., 60180 Nogent Sur Oise, France.

Measurement of Residual Stresses

The standard x-ray diffraction method for measuring residual stresses in metallic components was used. In this method, line shifts due to a uniform strain in the component are measured and then the stresses in the component are determined by a calculation involving the elastic constants of the material. Figure 32 is a schematic representation of a surface under a plain stress condition. By knowing the strain free inter planar spacing d and $d_{o,}$ the modulus of elasticity in a specific crystal direction, E, and Poisson's ratio in that crystal direction, ν, the two components of the biaxial principle stress can be obtained from Eq. (6) [13-15].

$$\frac{d-d_O}{d_O}=(\frac{1+\nu}{E})\sigma_\phi \sin 2\psi-\frac{\nu}{E}(\sigma_1+\sigma_2) \tag{6}$$

Measurements were made in an x-ray diffractometer equipped with a stress analysis module[7]. The residual stresses were measured at the inner face of the hole in the thinnest section since this location is expected to have the highest magnitude of residual stress. The part is measured at the inside round surface where the maximum residual stresses occur. This restricts the X-ray beam path as shown in Figure 33. The upper part of the ring will block some of the X-ray beam diffraction angles. Similarly, due to restrictions imposed by the part geometry, bi-axial stress analysis is difficult. Therefore, uni-axial residual stresses analysis is applied, which is the standard method for measuring large samples [15]. Figure 34 shows the peak (~157°) and angular range that was used for residual stresses analysis.

[7] Model X'Pert Pro Diffractometer manufactured by PANalytical, Inc., Natick, MA, USA.

Residual stress measurements on vertically and horizontally quenched parts are shown in Figure 35 and 36. A comparison between the measured and model- predicted magnitude of residual stress in the part is shown in Figure 37. It is clear that there is very good agreement between the measured and the model-predicted residual stresses and that quenching the part vertically creates more residual stresses in the part than quenching it horizontally. The residual stress measurements at maximum location are well matched to x-ray measurements. The accuracy is 94.2% for the vertically quenched part and 99% for the horizontally quenched part.

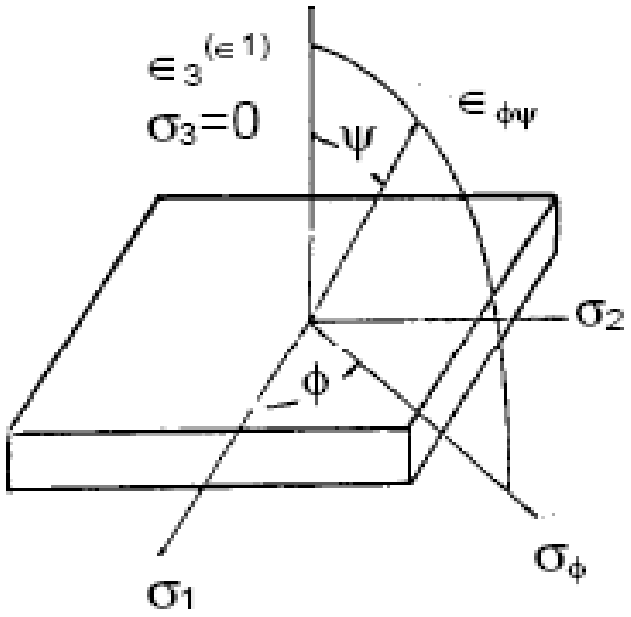

Figure 32. A schematic representation of a surface under plain stress. [14]

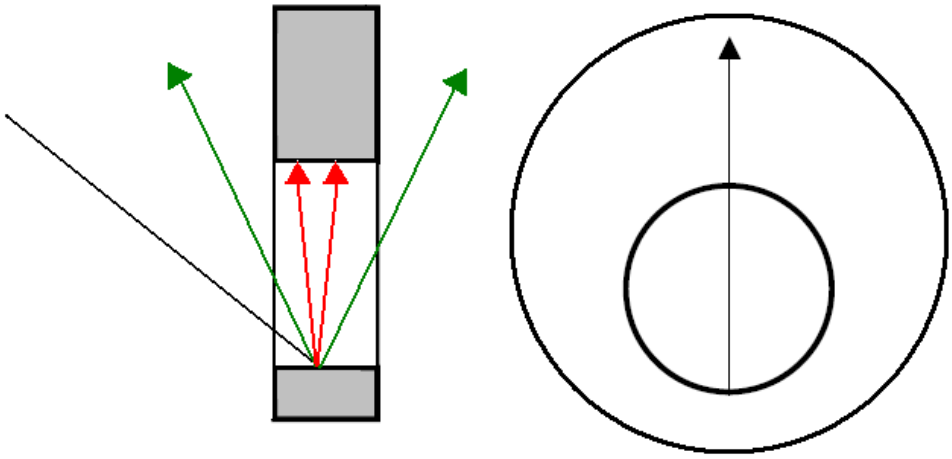

Figure 33. Diffractometer and location on the part where residual stresses were measured.

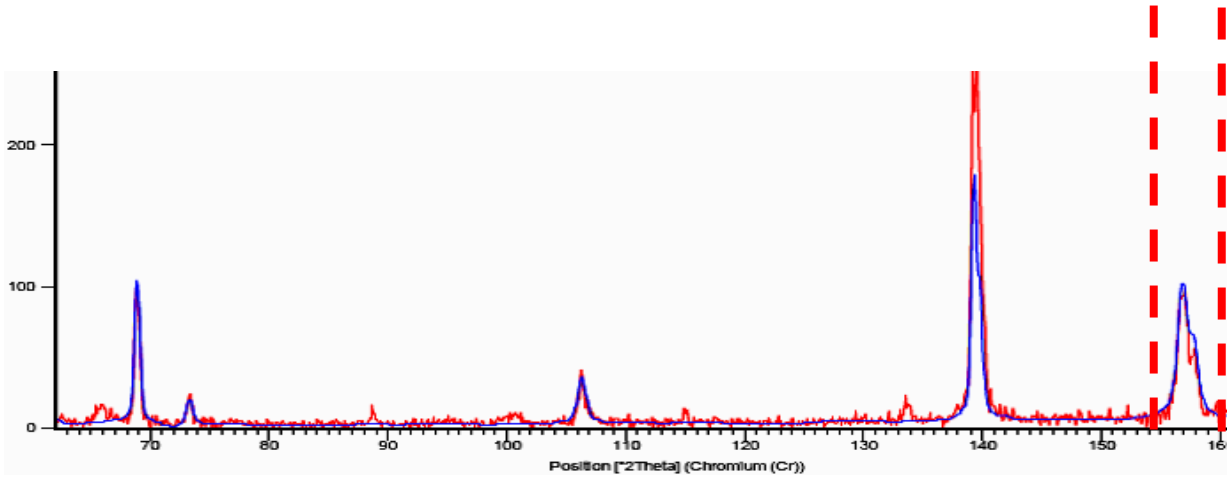

Figure 34. Diffraction pattern showing the angular range selected.

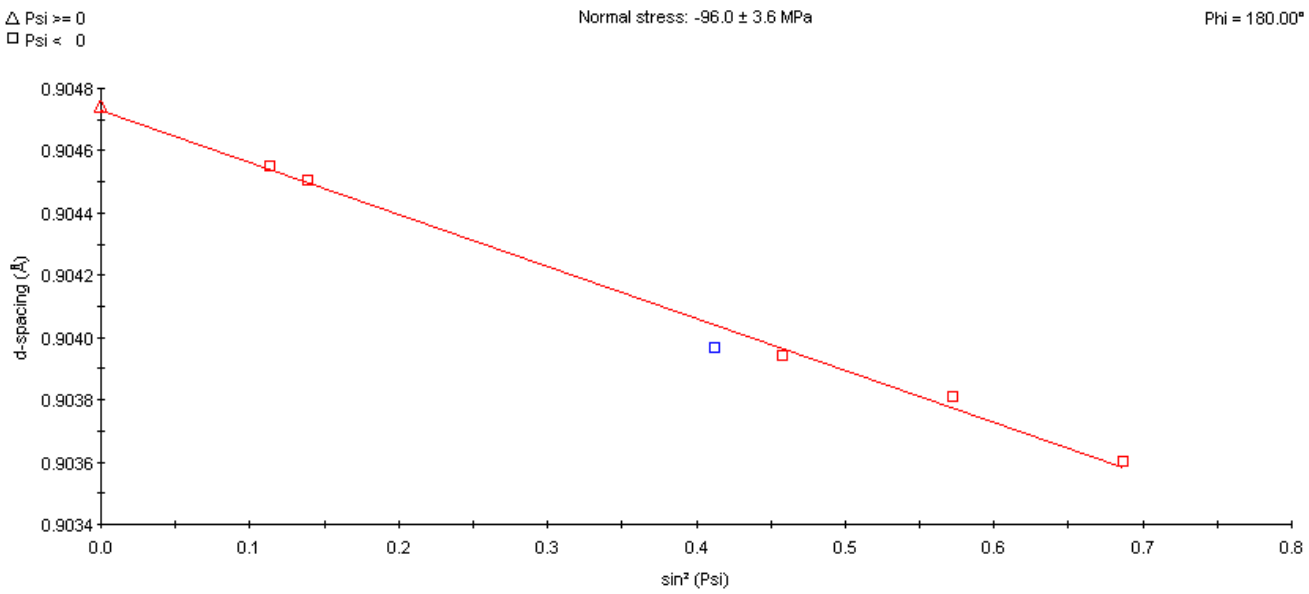

Figure 35. Change in d-spacing with $\sin^2\psi$ for the vertically quenched part.

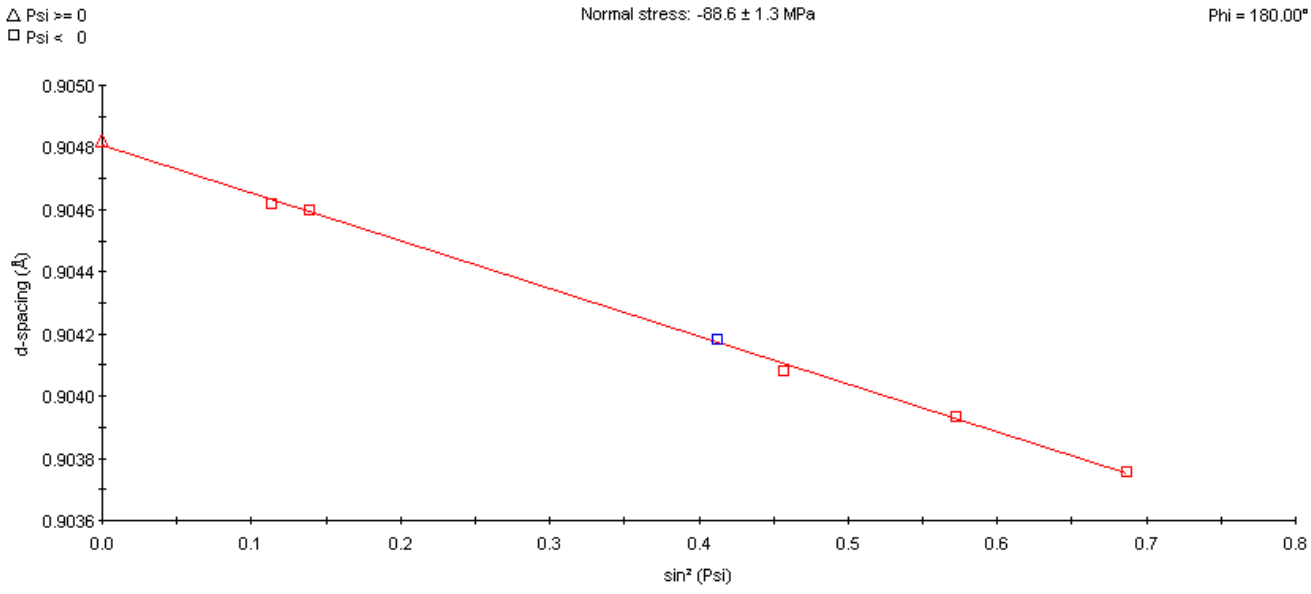

Figure 36. Change in d-spacing with sin2ψ for the horizontally quenched part.

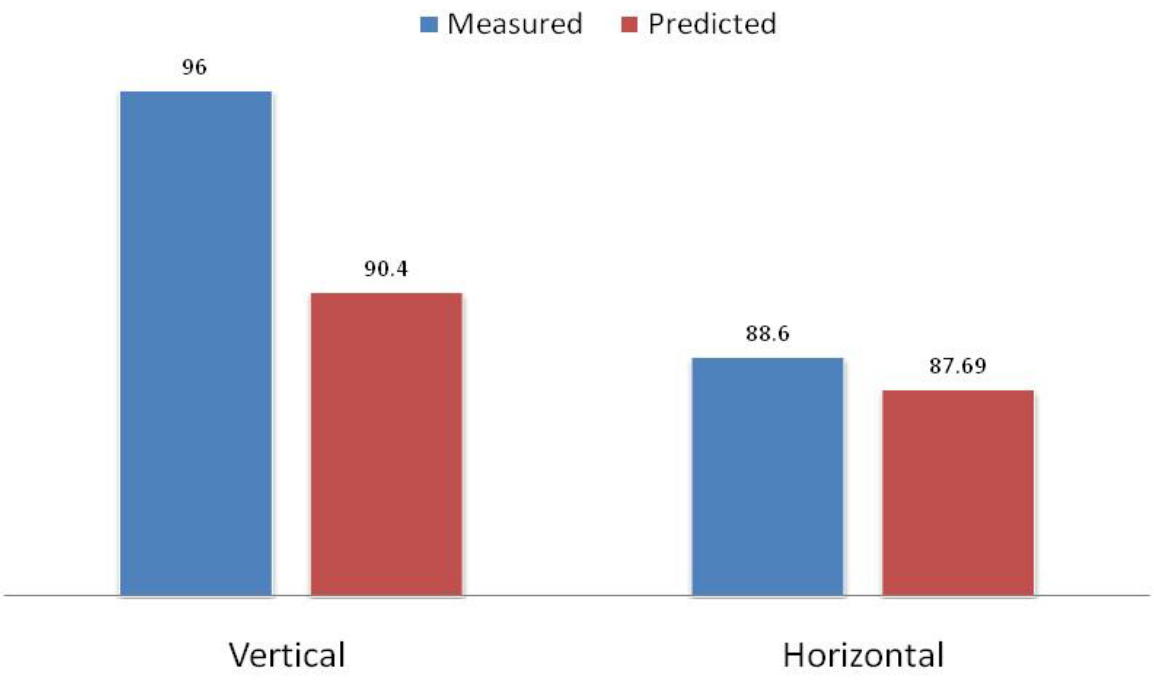

Figure 37. Measured vs. Predicted residual stresses in MPa.

Measurement of Dimensional Changes and Distortion

A Starrett coordinate measuring machine (CMM) was used to measure the dimensional changes and distortion caused by the heat treatment process. Sufficient measurements were made in order to obtain accurate representation of the part before and after heat treatment. In order to characterize the amount of distortion in the parts after heat treatment, a fixture was made to hold the rings at the same location in the CMM. The fixture was made out of an aluminum block with standard pins that fit the holes in the part to hold it in a vertical position with the thinnest section of the part pointing up. The middle circular hole is measured before and after heat treatment at locations around the periphery in 10° increments, started from the thickest section, as shown in Figure 38.

The CMM measurements were converted into a plot of angular radius change. Measured and model-predicted results are shown in Figure 39. There is good agreement between the measured and model-predicted distortion profiles. However, there is significant discrepancy in the magnitude of the distortion. Better temperature-dependent mechanical properties data is needed in order to improve the ability of the model to predict the magnitude of the distortion.

Figure 38. The path of CMM measurements.

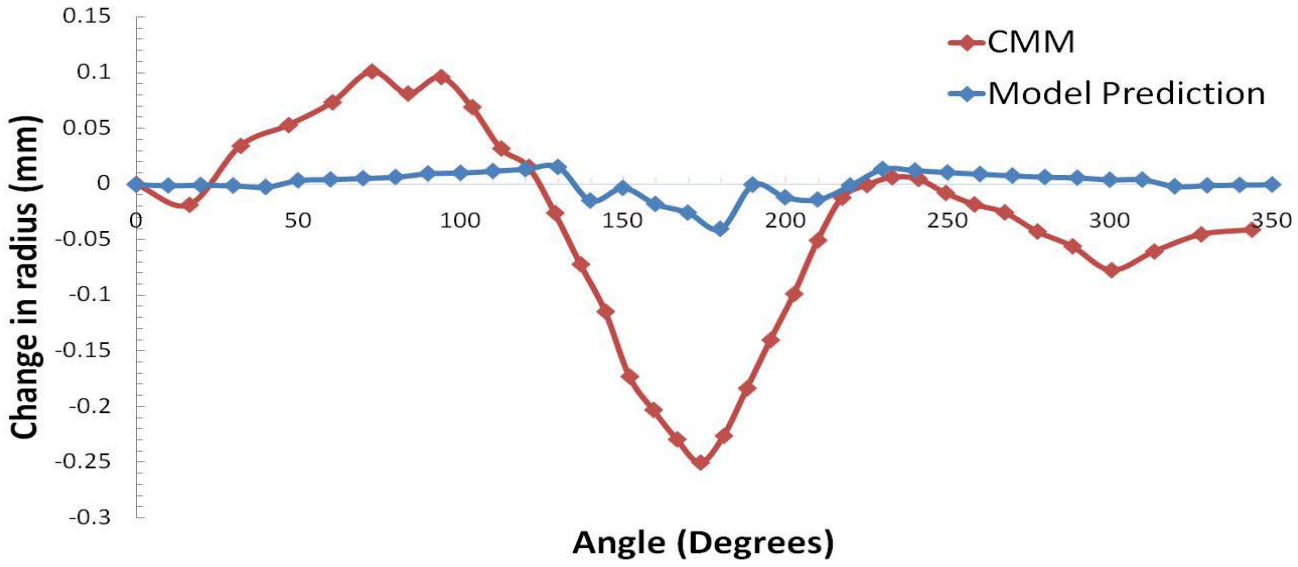

(a)

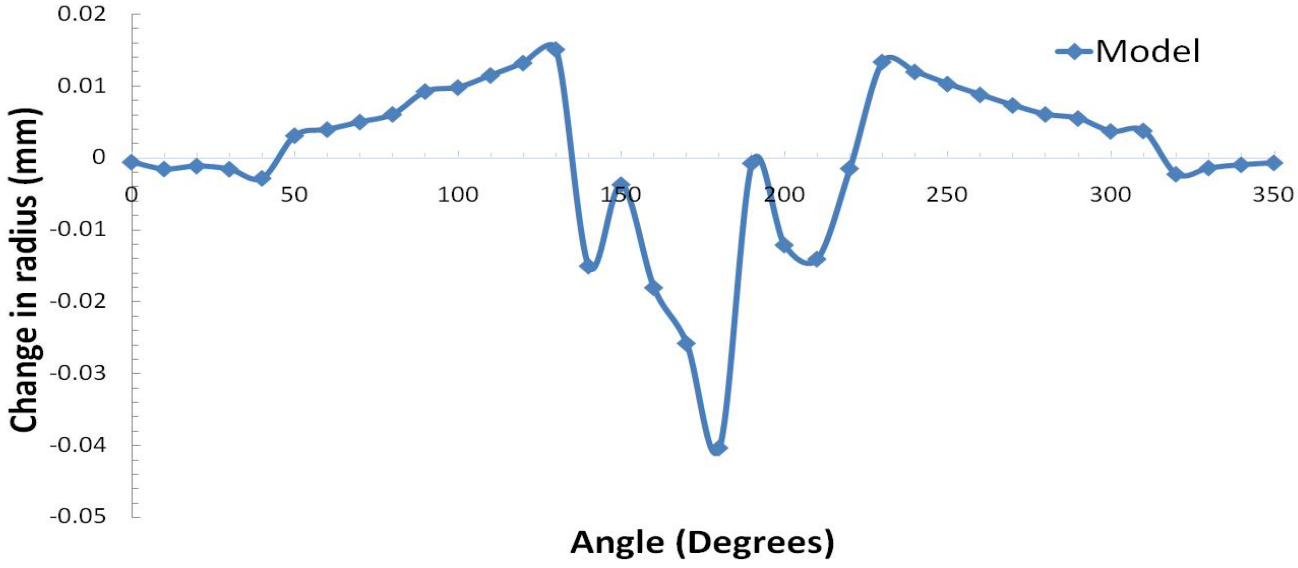

(b)

Figure 39. Measurements of the inner hole of the part (vertical quenching) for (a) CMM measurement vs. model prediction, (b) model prediction in different units.

The distortion measurements show that the model correctly predicts the location where the maximum distortion occurs, but the predicted distortion is consistently lower in magnitude than the measured distortion.

The in predicting the magnitude of distortion is attributed to the inaccuracy of the mechanical properties used in the stress module. It is believed that the tensile test bars used to measure the room and elevated temperature mechanical properties naturally aged during the measurements. This was particularly true in measurements performed at low strain rates and resulted in incorrect (higher) strength values for the supersaturated solid solution. It has been shown [16, 17] that independent self-clusters of Mg and Si atoms form in A356 alloy when it is held even for a relatively short time in the temperature range between -30℃ (-22°F) and 70℃ (158°F). The formation of these clusters is accompanied by an increase in hardness (VHN) from 53 to 68 after 1 hour of natural aging [18].

In order to further prove this concept, two specimens were tested: (1) One specimen was tested right after it was quenched, and (2) one specimen that was tested after being kept at room temperature for four hours after quenching. The results are shown in Figure 40. It is important to notice that the quenched A356 alloy is highly unstable and easily forms precipitates, even when held at room temperature. This experiment illustrates how easily supersaturated A356 alloy could naturally age. More accurate model predictions of deformation are believed to be attainable with a data base that accurately reflects the mechanical properties of the supersaturated alloy without natural aging effects.

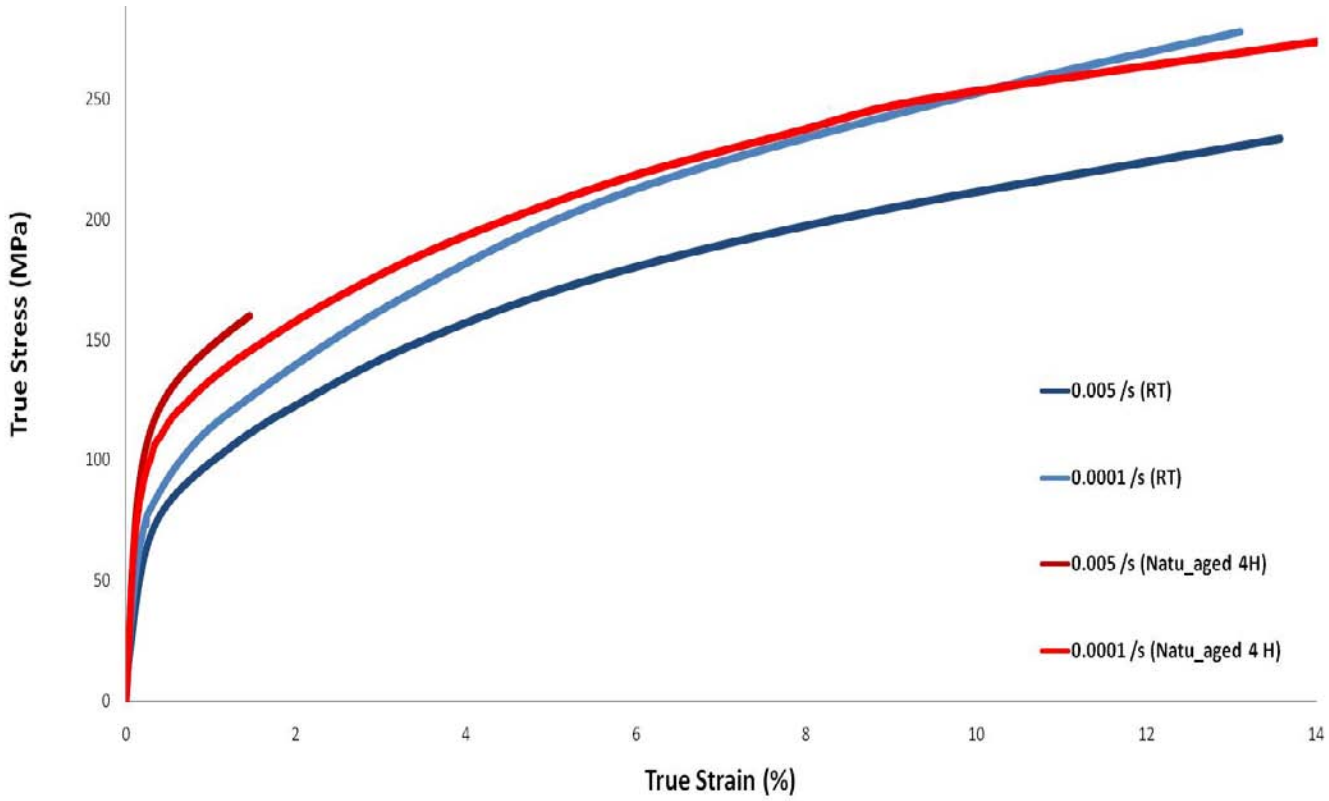

Figure 40. True stress-strain curves for supersaturated and naturally aged A356 alloy.

6. Summary and Conclusions

- A finite element model has been developed based on the commercially available software, ABAQUS (version 6.7.1) to predict the response of aluminum alloy castings to heat treatment. The model predicts the magnitude and sense of residual stresses and the magnitude and profile of distortion caused by the quenching step.

- The model was used to simulate the response of a commercially produced part to the standard T6 heat treatment. Residual stresses and distortion were measured on heat treated parts and compared to the computer predictions. Residual stress was measured with the standard x-ray method and distortion was measured with a coordinate measuring machine.

- The subroutine specially developed for this work allows the user of the model to define the quenching direction and quenching velocity.

- It was found that:

  - The predicted residual stresses are in good agreement with measurements.

  - Although the model correctly predicts the location of maximum distortion, predicted distortion magnitudes are significantly lower than the measured ones. It is believed that improved predictions are possible with a more accurate mechanical properties data base.

7. References

[1] Emadi D, Whiting, L.V., Sahoo, M., Sokolowski, J.H., Burke, P., and Hart, M. *Optimal heat treatment of A356.2 alloy*. Light Metals 2003:983.

[2] D.J. Bammann MLC, and G.C. Johnson. Modeling Large Deformation and Failure in Manufacturing Processes. *Proceedings of the Nineteenth International Congress on Theoretical and Applied Mechanics* 1996:359.

[3] Virendra S. Warke JY, Mohamed Maniruzzaman, Makhlouf M. Makhlouf, and Richard D. Sisson, Jr. Modeling the Heat Treatment of Powder Metallurgy Steels. *Proceedings of the 2004 International Conference On Powder Metallurgy and Particulate Materials, part-1,*. Chicago, IL, 2004. p.39.

[4] DANTE users mannual. Deformation Control Technology, Inc., 2003.

[5] Hibbitn KaS, Inc. Heat Transfer and Thermal-Stress Analysis with ABAQUS Training. 2002.

[6] V. S. Warke GTaMMM. Mathematical Modeling and Computer Simulation of Molten Metal Cleansing by the Rotating Impeller Degasser: Part I. Fluid Flow. J. Mater. Process. Tech. 2005;168:112.

[7] V.S. Warke SS, and M.M. Makhlouf. Mathematical Modeling and Computer Simulation of Molten Metal Cleansing by the Rotating Impeller Degasser: Part II. Removal of Hydrogen Gas and Solid Particles. J. Mater. Process. Tech. 2005. ;vol. 168:pp. 119.

[8] M. Maniruzzaman JCC, C. McGee, S. Ma and R.D. Sisson, Jr. CHTE Quench Probe System - a new quenchant characterization system. the 5th International Conference on Frontiers of Design and Manufacturing, ICFDM. Dalian, China, 2002

[9] C.A. Muojekwu IVSaJKB. Casting-chill Interface Heat Transfer during Solidification of an

Aluminum Alloy. *Metall. Mater. Trans* 1995;26:361.

[10] C.M. Estey SLC, D.M. Maijer & C. Hermesmann. Constitutive Behavior of A356 During The Quenching Operation. Mater. Sci. Eng 2004;A 383:245.

[11] Meckin UFKaH. Physics and Phenomenology of Strain. Hardening: The FCC Case. Prog. Mater. Sci. 2003;48:171.

[12] P. Li DMM, T.C. Lindley, and P.D. Lee. Simulating the Residual Stress in an A356 Automotive Wheel and its Impact on Fatigue Life. Metallurgical and Materials Transactions B 2007;38A:505.

[13] Stock BDCaSR. Elements of X-Ray Diffraction: *Princeton Hall Publications*, 2004.

[14] Prevey PS. A method of Determining Elastic Constants in Selected Crystallographic direction for X-Ray diffraction residual stress measurement. *Advances in X-Ray Analysis* 1977;20:345.

[15] Guley V. Residual stress and retained austenite X-Ray diffraction measurements on ball bearings. PANalytical Co., 2003.

[16] C.D. Marioara SJA, J. Jansen and H. W. Zandbergen. The influence of temperature and storage time at RT on nucleation of the β" phase in a 6082 Al-Mg-Si alloy. Acta Materialia 2003;51:789.

[17] G. A. Edwards KS, G. L. Dunlp and M. J. Couper. The precipitation sequences in Al-Mg-Si alloys. Acta Materialia 1998;46:3983.

[18] H. Moller GG, W. E. Stumpf Investigation of the T4 and T6 Heat Treatment Cycles of Semi-Solid Processed Aluminium Alloy A356 The Open Materials Science Journal 2008;2:11.